LIMNOLOGY and OCEANOGRAPHY

ASLO

Limnol. Oceanogr. 66, 2021, 807–826

doi: 10.1002/lno.11644

Coastal hypoxia and eutrophication as key controls on benthic release and water column dynamics of iron and manganese

Wytze K. Lenstra,[1*] **Martijn Hermans**,[1] **Marie J.M. Séguret**,[1] **Rob Witbaard**,[2] **Silke Severmann**,[3] **Thilo Behrends**,[1] **Caroline P. Slomp**[1]

[1]Department of Earth Sciences—Geochemistry, Utrecht University, Utrecht, The Netherlands
[2]Department of Estuarine and Delta Systems, NIOZ, Royal Netherlands Institute for Sea Research and Utrecht University, Yerseke, The Netherlands
[3]Department of Marine and Coastal Science, Rutgers, The State University of New Jersey, New Brunswick, New Jersey

Abstract

Continental shelves are a major source of iron (Fe) and manganese (Mn) to marine waters. Here, we investigate controls on benthic release of Fe and Mn and the impact on the water column in the Baltic Sea. We find high in situ benthic release rates of dissolved Fe and Mn at seasonally hypoxic sites (bottom water oxygen between 0–63 μmol L^{-1}) receiving high inputs of organic matter. We find that benthic Fe and Mn release is sensitive to bottom water oxygen concentrations. Benthic Fe release is likely additionally controlled by Fe–sulfur redox chemistry in the surface sediment. For Mn, benthic release correlates positively with Mn oxide availability in the surface sediment. Benthic release contributes to high dissolved Fe and Mn concentrations in the water column and is amplified by repeated cycling of Fe and Mn between the sediment and overlying water through benthic release, oxidation in the water column, deposition as metal oxides, followed by reductive dissolution. Most water column Fe (~ 80%) is present in particulate form near the seafloor. In contrast to Fe, a large percentage of the Mn remains dissolved (~ 50%). We show that easily reducible Fe and Mn oxides are key forms of particulate Fe and Mn in suspended matter. The Baltic Sea represents a highly eutrophic, low oxygen end-member when compared to other modern coastal systems. Our results imply that, upon continued eutrophication and deoxygenation of the coastal ocean, benthic release of dissolved Fe and Mn from continental shelves could become greater than previously thought.

Iron (Fe) and manganese (Mn) are essential nutrients for phytoplankton (Moore et al. 2013). Release from sediments and subsequent lateral transport of Fe and Mn over continental shelves, which is termed "shuttling", is a key source of Fe and Mn to the open ocean (Lyons and Severmann 2006; Raiswell and Canfield 2012). The shuttling of Fe and Mn also impacts the lateral transport and sedimentary sequestration of phosphorus (P) and trace metals (e.g., cobalt and molybdenum) (Dellwig et al. 2010; Jilbert and Slomp 2013). Insight into the processes that control benthic release of Fe and Mn and their fate in the water column is key to understanding the role of continental shelves as a source of trace metals and nutrients to the ocean.

Production of dissolved Fe and Mn in sediments through reductive dissolution of Fe and Mn oxides is driven by the degradation of organic matter and associated sulfide production (Burdige 2006). Part of the dissolved Fe and Mn may precipitate in the sediment forming authigenic minerals, such as Fe sulfides (Berner 1984) and Mn carbonates (Burdige 1993). Part of the dissolved Fe and Mn can be released to the overlying water and this release is most pronounced for sediments under oxygen-depleted, and for dissolved Fe, non-sulfidic bottom waters (Pakhomova et al. 2007; Homoky et al. 2011; Scholz et al. 2014). In sediments overlain by oxic bottom waters, bioirrigating macrofauna can contribute to benthic release of dissolved Fe and Mn (Berelson et al. 2003; Lenstra et al. 2019). Because the oxidation of dissolved Mn(II) and Mn(III), which is mainly bacterially mediated, is slower than that of dissolved Fe(II) (Stumm and Morgan 1996; Learman et al. 2011), more porewater Mn than Fe is expected to reach

*Correspondence: w.k.lenstra@uu.nl

Additional Supporting Information may be found in the online version of this article.

Author Contribution Statement: W.L. and C.S. designed the research. W.L., M.H., M.S., and T.B. performed the analyses. W.L., M.H., M.S., R.W., S.S., C.S. performed the fieldwork. W.L., M.H., T.B., and C.S. interpreted the data. W.L. and C.S. wrote the paper with comments provided by M.H., M.S., T.B., and S.S.

the overlying water (Thamdrup et al. 1994*b*; Slomp et al. 1997). Under complete and persistent depletion of oxygen, benthic release of dissolved Fe and Mn is usually low because of limited deposition of reducible Fe and Mn oxides at the sediment water interface (Slomp et al. 1997; Wijsman et al. 2001).

Dissolved Fe and Mn released from sediments into oxygenated overlying waters may precipitate as Fe and Mn oxides (Emerson et al. 1982; Millero et al. 1987). These metal oxides can remain suspended or can settle to the seafloor, often leading to a cycle of deposition at the sediment–water interface, mobilization in dissolved form in the sediment, escape to the overlying water and oxidation upon contact with oxygen followed by redeposition. This type of recycling that includes the water column is termed "refluxing" (Adelson et al. 2001). In the presence of dissolved organic matter, dissolved Fe(II) and Mn(II) can also be oxidized to Fe(III) and Mn(III) and complexed with organic ligands and stay in solution (Gledhill and van den Berg 1994; Oldham et al. 2017*b*). While in marine environments organically complexed Fe (Fe(III)-L) is typically colloidal (0.2–0.02 μm; Eckert and Sholkovitz (1976); Schlosser et al. (2013)), organically complexed Mn (Mn(III)-L) is aqueous (< 0.02 μm; Oldham et al. (2017*a*)). Both dissolved and particulate Fe and Mn in continental shelf waters can be transported laterally and contribute to metal transport from continental shelves to adjacent deeper basins or open ocean waters (Noble et al. 2012). However, the relative contributions of particulate vs. dissolved forms of Fe and Mn to this transport are still incompletely understood.

Many coastal areas worldwide are suffering from increased eutrophication and deoxygenation of bottom waters (Diaz and Rosenberg 2008; Breitburg et al. 2018). A decline in bottom water oxygen typically initially leads to enhanced benthic release of dissolved Fe and Mn from sediments because of less efficient transformation to metal oxides in surface sediments (Sundby et al. 1986; Slomp et al. 1997; Elrod et al. 2004), with fluxes amplified by refluxing (Adelson et al. 2001; Lohan and Bruland 2008; Sulu-Gambari et al. 2017). However, in sediments with high rates of organic matter input, sulfate reduction and associated sulfide production, porewater Fe may precipitate as Fe sulfides and, despite low bottom water oxygen, little dissolved Fe may escape to the overlying water. The concept of this "redox window" for benthic Fe release has been deduced from sediment records (Scholz et al. 2014; Lenz et al. 2015*a*). However, the increased retention of dissolved Fe at low oxygen because of an increased availability of dissolved sulfide is not captured in sensitivity studies of shelf release of dissolved Fe as a function of organic matter oxidation and/or bottom water oxygen using reactive transport models (Elrod et al. 2004; Dale et al. 2015) nor in empirical functions developed for ocean biogeochemical models (Elrod et al. 2004; Dale et al. 2015). These latter functions specifically link benthic Fe release to carbon oxidation rates in sediments. For benthic release of dissolved Mn, a similar redox window is not expected, given the higher mobility of dissolved Mn in sulfidic waters compared to dissolved Fe. Instead, the input of Mn oxides from the overlying water (Thamdrup et al. 1994*a*; Slomp et al. 1997) or upward diffusive fluxes from deeper sediment layers may control benthic fluxes of dissolved Mn (e.g., Heiser et al. (2001); Pakhomova et al. (2007)).

The Baltic Sea is highly suitable for studies of the consequences of severe eutrophication and deoxygenation on Fe and Mn dynamics in coastal seas, given the intensity of recent changes in bio-geochemistry induced by human activities (Conley et al. 2009; Reusch et al. 2018). Sediment records of Fe in the anoxic and sulfidic (euxinic) deep basins of the Baltic Sea indicate that the expansion of the area of low oxygen led to a period of enhanced Fe shuttling to the deep basins between the early 1970s and mid-1990s, with a peak around 1981 (Lenz et al. 2015*a*; Reed et al. 2016). The waning of the strength of the Fe shuttle from the 1990s onwards was attributed to increased retention of Fe as Fe sulfides in the source regions around the deep basins.

In this study, we assess the benthic release of dissolved Fe and Mn and its impact on the water column at nine sites with a range of bottom water oxygen concentrations and rates of sulfate reduction in the sediment. We focus on three areas of the Baltic Sea that could potentially act as a source of Fe to the deep basins, namely the Gulf of Finland, Gotland area and two Southern basins, Bornholm and Arkona. We combine porewater and sediment depth profiles and in situ benthic flux measurements of Fe and Mn with water column analyses of dissolved and particulate Fe and Mn. We find the highest rates of benthic release of Fe and Mn at sites with hypoxic bottom waters (bottom water oxygen between 0 and 63 μmol L^{-1}) and strong refluxing of metals through release and deposition cycles involving the water column. Sulfide availability in porewaters (for Fe) and Mn oxide supply likely act as additional controls.

Methods

Study area and sampling

The Baltic Sea is a semi-enclosed brackish basin characterized by high rates of organic matter production, low bottom water oxygen concentrations and low macrofaunal densities (Conley et al. 2009). Our study sites are located in three different areas: the Gulf of Finland (sites LL3A, GOF5 and JML), the Gotland area (sites LF1, 311, BY15, and LL19) and the Southern basins (sites BY2 and BY5; Fig. 1; Table 1).

The Gulf of Finland is the most eutrophic region of the three investigated areas (Andersen et al. 2015). In this region, we sampled three seasonally hypoxic sites where hypoxia is defined as a bottom water oxygen concentration between 0 and 63 μmol L^{-1}. Two sites (LL3A and GOF5) are characterized by a distinct yearly cycle in bottom water oxygen, while the third site (JML) is only briefly oxygenated in winter (Table 1; Hermans et al. (2019*a*)). The Gotland area features a permanent halocline between 70 and 80 m water depth.

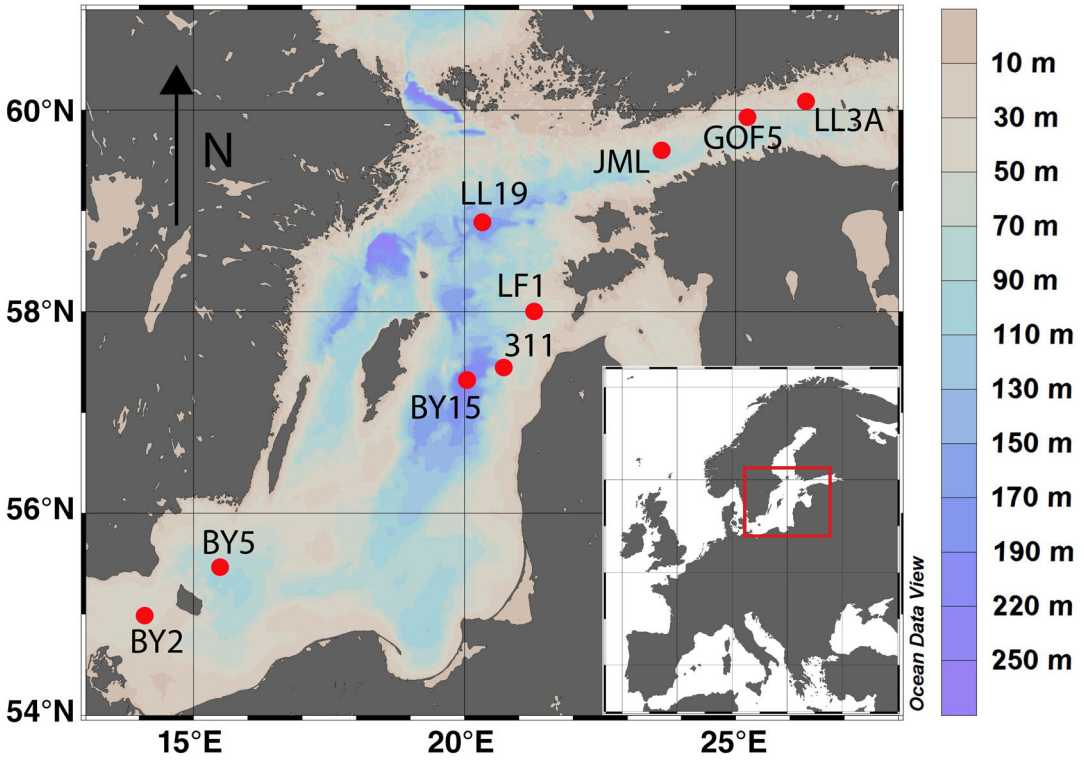

Fig. 1. Locations of the nine sites sampled in the Baltic Sea in June 2016 (Table 1). The sample sites are located in the Gulf of Finland (JML, GOF5, and LL3A), Gotland basin area (LF1, 311, BY15, and LL19) and Southern basins (BY2 and BY5).

Restricted ventilation of the deep water below the halocline contributes to euxinia below this depth (Andersen et al. 2015). While bottom waters at LL19 have been euxinic for more than a decade (Lenz et al. 2015*b*), those at site BY15 were recently reoxygenated due to two inflow events of saline and oxygen-rich water from the North Sea in December 2014 and November 2015 (Mohrholz et al. 2015; Hermans et al. 2019*b*). The inflow pushed anoxic waters from the deep basin onto the adjacent shelf where the seasonally hypoxic sites LF1 and 311 are located, contributing to a decline in bottom water oxygen (Hermans et al. 2019*b*). The inflow also led to a rise in bottom water oxygen at the generally hypoxic site in the Bornholm basin, BY5, and the seasonally hypoxic site in Arkona basin, BY2.

Water column and sediment samples were collected at all nine sites during a cruise with R/V *Pelagia* in June 2016. Water

Table 1. Coordinates, water depth, bottom water temperature, salinity and classification based on bottom water oxygen and H_2S between 2014 and 2016 (Hermans et al. 2019*a*) for the nine sites sampled in the Baltic Sea. Unit mbss is meters below sea surface. Macrofaunal density (individuals m^{-2}) were taken from Hermans et al. (2019*a*).

Site		Latitude (N)	Longitude (E)	Depth (mbss)	Temperature (°C)	Salinity	Macrofaunal density (ind m^{-2})	Classification
LL3A	Gulf of Finland	60°4.43′	26°18.30′	60	5	8.9	1007±734	Seasonally hypoxic
GOF5	Gulf of Finland	59°57.10′	25°11.02′	65	5.1	9.4	1227±249	Seasonally hypoxic
JML	Gulf of Finland	59°35.32′	23°37.50′	80	5.7	10.7	n.a.	Seasonally hypoxic*
LF1	Gotland area	57°59.35′	21°17.24′	67	4.8	8.4	625±113	Seasonally hypoxic
311	Gotland area	57°26.49′	20°43.49′	65	5.5	10.1	301±104	Seasonally hypoxic
BY15	Gotland area	57°19.20′	20°3.0′	237	7.5	13.8	0	Reoxygenated
LL19	Gotland area	58°53.24′	20°19.5′	173	6.2	11.7	0	Euxinic
BY5	Bornholm basin	55°28.09′	15°29.13′	87	6.8	18.4	1361±705	Reoxygenated
BY2	Arkona basin	54°58.50′	14°5.37′	47	7	16.5	1694±593	Seasonally hypoxic

*The JML site is likely in transition towards permanent euxinia.

column depth profiles of conductivity, temperature, density and dissolved oxygen were obtained with a CTD (Conductivity-Temperature-Density) profiler equipped with a polarographic membrane oxygen sensor (Seabird Scientific SBE43). Water column samples were collected using a TITAN-CTD frame, with 24 ultraclean sampling bottles of 24 liter, each made of polyvinylidene fluoride and titanium (PVDF) (Rijkenberg et al. 2015). After deployment the ultraclean CTD system was moved to a Class-100 container for subsampling. Suspended matter in the water column was collected through in situ pumping at all sites except at GOF5 and 311. Sediment cores were collected with an Oktopus multicorer (inner diameter: 10 cm) using polycarbonate tubes of 60 cm length. Only sediments with a minimum of 10 cm overlying water and an intact sediment surface were processed further. At all sites, two bottom water samples were taken directly after core retrieval. One sediment core was sliced into intervals of 0.5–3 cm under a nitrogen atmosphere at bottom water temperature (Table 1). Each slice was divided over a pre-weighed glass vial and a 50 mL centrifuge tube. The glass vials were stored under a nitrogen atmosphere at −20°C for solid phase analyses onshore. The 50 mL centrifuge tubes were centrifuged on board at 4500 rpm for 25 min to extract porewater. In situ benthic flux measurements of dissolved Fe, dissolved Mn and oxygen were carried out with an Albex lander at all sites except JML.

Water column analyses

Water column samples for analysis of hydrogen sulfide (H_2S: sum of H_2S, HS^-, and S^{2-}) were filtered over 0.2 μm acrodisc filters. Subsequently, 1.5 mL of 8 mmol L^{-1} NaOH was added to 0.5 mL of sample to keep dissolved sulfide in the samples in the HS^- form (Kraal et al. 2017). Unfiltered samples for total dissolvable Fe and Mn (henceforth termed total Fe and Mn) were taken from the PVDF samplers using acid-washed LDPE tubing. The difference between total and dissolved Fe and Mn is assumed to be particulate. Samples for dissolved Fe and Mn (containing colloidal and aqueous Fe and Mn) were obtained using 0.2 μm Sartobran 300 cartridge filters (Sartorius). To avoid carry-over between samples, the first 0.5 liter of each filtered sample was discarded. Samples for aqueous Fe were filtered through 0.02 μm Virosart cartridge filters (Sartorius). Nitrogen pressure was applied at the top of the sampler and the samples were collected in acid-washed 60 mL LDPE bottles (Nalgene). Samples were acidified to pH 1.8 by adding 120 μL of distilled 10 M HCl to 60 mL of sample. Samples were stored at 4°C until analysis.

Samples for H_2S were analyzed on board with a Quattro gas-segmented continuous flow analyzer using the methylene blue method following Grasshoff et al. (2009). The concentration of Fe in all samples was determined on land by flow injection chemiluminescence with preconcentration detection (Klunder et al. 2011). The concentration of Mn was determined on land by Inductively Coupled Plasma Mass Spectrometry (ICP-MS; Nexion ICP-MS [Perkin Elmer]) after pre-concentration with a SC-DX SeaFAST S2 (Elemental Scientific). Acidified samples (pH 2) were buffered online with a pre-cleaned buffer solution (4.8 M glacial acetic acid 99.7% (Baseline, Seastar) and 4.1 M ammonium hydroxide 29% (Baseline, Seastar), pH 6) and loaded onto the pre-concentration column for 20 s (Lagerström et al. 2013). A detailed description of the Fe and Mn analysis of the water column samples is given in the supplement (Section S1).

In situ pumping to collect suspended matter was performed for 1–4 h at 4 water depths per site using four McLane pumps (×3 WTS-LV, ×1 WTS-LV Dual Filter). After retrieval of the pumps, residual water in the filter head was removed by vacuum pumping and the filters (Supor, 0.8 μm, 142 mm diameter) were placed in petri-dishes, sealed in plastic bags and stored at −20°C. In situ filters from anoxic depths were stored under a nitrogen atmosphere at −20°C. Iron in the suspended matter was determined on a quarter of every filter using a 4-step sequential extraction procedure targeting the following phases (Table S1): (1) ferrihydrite, (2) easily reducible Fe(III) and Fe(II) minerals, (3) reducible (crystalline) Fe oxides, and (4) magnetite. Step (1) was taken from Raiswell et al. (2010), Steps (2)–(4) are based on Poulton and Canfield (2005) and Claff et al. (2010). After extraction, all solutions were filtered through 0.45 μm pore size filters prior to analysis. Total Fe in the extraction solutions was determined colorimetrically using the 1,10-phenanthroline method (APHA 2005). In the 1 M HCl solution, both Fe(II) and total Fe were measured and Fe(III) was calculated by extracting the Fe(II) pool from total Fe. Total Mn concentrations in the extraction solutions were determined using a mixed ammonia/formaldoxime reagent, following (Brewer and Spencer 1971). Because of the potential interference of Fe during colorimetric Mn determination (Brewer and Spencer 1971), samples where Mn concentrations were higher than 0.6 μmol L^{-1} were analyzed by Inductively Coupled Plasma Optical Emission Spectroscopy (ICP-OES; Spectro Arcos). Similar to Fe, the Mn minerals that are dissolved are expected to decrease in reactivity from steps 1 to 4 (Table S1). The sum of all Mn phases extracted was assumed to represent reactive Mn (i.e., the sum of Mn oxides and Mn carbonates; Lenstra et al. (2020)).

Porewater analyses

At all sites, high-resolution depth profiles (50 μm) of dissolved oxygen were obtained from a separate intact sediment core directly after retrieval with a motor controlled 2D-micromanipulator and micro-electrodes (tip size 50 μm; Unisense A.S., Denmark). Calibration was performed with a 2-point calibration with 100% oxygen saturated and nitrogen purged artificial seawater, using the CAL300 calibration chamber (Unisense). Porewater was filtered under a nitrogen atmosphere through 0.45 μm pore size filters. After filtration a 0.5 mL subsample for H_2S analysis was immediately transferred into a glass vial containing 1.5 mL of 8 M NaOH

solution. A subsample of 0.15 mL was diluted in 1.35 mL of de-oxygenated UHQ water for SO_4^{2-} analysis. Subsamples for dissolved Fe and Mn and Na^+ were acidified with 10 μL 10 M suprapur HCl per mL of porewater. A subsample of 0.5 mL was transferred to a 4.9 mL glass vial to which 4.4 mL of 25 g L^{-1} NaCl solution was added, making sure that no headspace remained, for analysis of DIC. Aliquots of the remaining porewater were used to measure NH_4^+. At sites LF1, 311, BY5, and BY2 porewater was additionally filtered through 0.2 μm pore size filters and at site BY2 also through 0.02 μm filters to discern between 0.45–0.2 μm, 0.2–0.02 μm (colloidal), and < 0.02 μm (aqueous) Fe (Homoky et al. 2011; Raiswell and Canfield 2012). All subsamples were stored at 4°C and brought to room temperature prior to analysis.

Porewater samples for NH_4^+, DIC, and H_2S were analyzed on board with a Quattro gas-segmented continuous flow analyzers. Ammonia was determined following the indophenol blue method (Koroleff 1969), DIC after being oxidized by H_2O_2 following Stoll et al. (2001) with a precision of 8.7 μmol L^{-1} and H_2S following the methylene blue method (Grasshoff et al. 2009). Porewater samples for SO_4^{2-} were analyzed by ion-chromatography and total Fe, Mn and Na were analyzed by ICP-OES. Concentrations of < 0.02 and < 0.2 μm filter fractions for Fe were determined colorimetrically by the phenanthroline method following (APHA 2005).

Diffusive fluxes of dissolved Fe and Mn across the sediment–water interface (J in mmol m^{-2} d^{-1}) were calculated using Fick's first law of diffusion taking into account porosity, ambient salinity, pressure and temperature at each site using the R package CRAN: marelac (Soetaert et al. 2010).

Analysis of lander samples and in situ flux calculations

Benthic oxygen uptake and fluxes of dissolved Fe and Mn across the sediment–water interface were determined in situ with a benthic lander, equipped with three chambers made of the inert plastic Delrin, each with a surface area of 144 cm^2 and a volume of overlying water of 0.9 to and 2.6 liter (Tables S2–S9). A detailed description of the benthic lander and sample analysis is given in Section S2.

Fe was determined through flow injection chemiluminescence and Mn by ICP-MS after preconcentration with a SC-DX SeaFAST S2 as described for the water column samples. Fluxes of Fe and Mn across the sediment–water interface were determined by fitting a linear regression to the concentration time series from each chamber (after correction for the dilution with the bottom water at each sampling interval). Only regressions with $R^2 > 0.5$ were considered (Figs. S2, S3). Calculated Fe and Mn fluxes for the different incubation chambers were averaged for each site. Oxygen uptake was determined by fitting a linear regression line through all data points at all sites. However, because of low oxygen concentrations this could only be determined at GOF5, LL19, LF1, BY2, and BY5 (Fig. S4).

Solid phase analyses and sulfate reduction rates

All sediments were freeze-dried and the porosity was determined from the weight loss upon freeze drying. Freeze-dried sediments were ground in an agate mortar inside an argon purged glovebox and separated into an oxic and anoxic fraction. Speciation of solid phase Fe and sulfur (S) was determined on the anoxic subsamples to avoid oxidation artifacts (Kraal et al. 2009). All other analyses were performed on oxic subsamples.

To determine the total elemental concentrations of aluminum (Al), Fe, Mn and S, ca. 125 mg of sediment was digested in 2.5 mL mixed acid (HNO_3 : $HClO_4$; 2 : 3) and 2.5 mL 40% HF at 90°C. After fuming off the acids, the residue was redissolved in 4.5% HNO_3. The solutions were subsequently analyzed with ICP-OES. The analytical uncertainty (standard deviation) based on duplicate and triplicate analyses was < 2% for Al, < 3% for Fe, < 3% for Mn, and < 4.5% for S. A second subsample of ca. 300 mg was decalcified with two wash steps of 1 M HCl and subsequently dried, powdered and analyzed for carbon (C) using an elemental analyzer (Fisons Instruments model NA 1500 NCS). Organic C content was determined after correction for the weight loss following decalcification. The analytical uncertainty based on duplicates and triplicates was < 1%. A third subsample of ca. 50 mg was subjected to steps (2)–(4) of the sequential extraction procedure for Fe as described for suspended matter (Table S1). Average analytical uncertainty, based on duplicates, was < 4% for all fractions. A fourth subsample of ca. 500 mg was subjected to a sequential S-extraction according to Burton et al. (2006). This extraction was carried out in two steps (Table S1): (2.1) acid-volatile sulfur (AVS, i.e., mostly FeS) for 24 h by addition of 2 mL of ascorbic acid and 10 mL of 6 M HCl to the sediment and trapping of the released H_2S into a tube filled with 7 mL Zn-acetate; subsequently elemental sulfur (S0) was removed overnight with 25 mL methanol; (2.2) chromium-reducible sulfur (CRS, i.e., mostly FeS_2) for 48 h by addition of acidic chromium chloride solution and trapping of the released H_2S into a tube filled with 7 mL Zn-acetate. Samples for AVS and CRS were analyzed by iodometric titration of the alkaline Zn-acetate trap, following APHA (2005). The analytical uncertainty based on duplicates was < 5% for AVS, and < 10% for CRS. All solid phase measurements were corrected for the salt content based on the gravimetric water content and porewater Na^+ concentrations (Fig. S5).

At all sites sulfate reduction rates were determined on a separate sediment core according to Fossing and Jørgensen (1989).

Results

Site characteristics

At our nine study sites, bottom water temperature ranged from 4.8°C to 7.5°C (Table 1). Bottom water salinity decreased with increasing distance from the North Sea and with decreasing water depth. Macrofauna were present at all seasonally

hypoxic sites sampled and at one of the reoxygenated sites and were most abundant in the Southern basins (BY5 and BY2), at densities of up to ca. 1700 individuals m^{-2} (Table 1). Macrofauna were absent in sediments below the halocline in the Gotland area (BY15 and LL19). At the time of sampling, bottom water oxygen concentrations were in the hypoxic range (0–63 μmol L^{-1}) at six sites. Bottom water oxygen was absent at two sites (LL19, JML; Table 2). Oxic bottom waters were only observed at one of the Southern basin sites (BY2).

Surface sediments were typically highly enriched in organic carbon (> 5 wt%), with the exception of sites LF1 and 311 where concentrations were lower (3.5 and 1.1 wt%, respectively). Sediment oxygen uptake ranged from 0 to 7.7 mmol m^{-2} d^{-1} (Fig. S4; Table 2). Oxygen penetration depths varied between 0 and 3.5 mm (Fig. S6; Table 2). Sulfate reduction rates, integrated with depth, ranged from 0.24 to 2.5 mmol m^{-2} d^{-1} and were highest in the Gulf of Finland (Fig. S7; Table 2).

Porewater profiles and benthic release of dissolved Fe and Mn

Porewater NH_4^+ and DIC concentrations increased with depth at all sites and were highest in the Gulf of Finland (up to 650 μmol L^{-1} and 12 mmol L^{-1}, respectively; Fig. 2). Porewater concentrations of SO_4^{2-} always decreased with depth but complete SO_4^{2-} removal within 15 cm was only observed at the Gulf of Finland sites LL3A and JML. Porewater H_2S was present at all sites, but concentrations were again highest in the Gulf of Finland, with values up to 2000 μmol L^{-1}. At most sites, porewater Fe and Mn were elevated close to the sediment–water interface and decreased below a depth of 5 cm. Where this was not the case, concentrations were mostly constant at depth. The only exception was site LL19 where Mn concentrations increased with depth. Concentrations of dissolved Fe were highest at sites LF1, 311 and BY2 (> 140 μmol L^{-1}). Concentrations of dissolved Mn were highest at sites LL3A, GOF5 and BY15 (> 330 μmol L^{-1}). Dissolved Fe occurred in the porewater predominately in aqueous and/or colloidal form (< 0.2 μm; Fig. S8). The contribution of the 0.2 to 0.45 μm size fraction ranged from 4% to 22%, and varied between sites. At site BY2, aqueous (< 0.02 μm) Fe accounted for between 75% and 40% of total porewater Fe.

In situ benthic release of dissolved Fe was highest at sites LL3A, 311 and BY5, at rates of 1.21, 2.6, and 0.72 mmol m^{-2} d^{-1}, respectively. At the other sites, fluxes were below 0.4 mmol m^{-2} d^{-1} (Fig. 3; Table 3). In situ benthic release of dissolved Mn was highest at sites LL3A, GOF5, BY15 and BY5, at rates of 3.7, 6.6, 15.3, and 2.0 mmol m^{-2} d^{-1}, respectively. At the other sites fluxes were below 0.2 mmol m^{-2} d^{-1} (Fig. 3; Table 3). Diffusive fluxes calculated from the porewater profiles of dissolved Fe and Mn typically did not directly match with measured in situ fluxes (Table 3), likely because of a lack of appropriate depth resolution of our porewater sampling (Dale et al. 2015; Lenstra et al. 2019).

Solid phase Fe and Mn

Surface sediments were enriched in easily reducible Fe oxides at all sites except LL19 (Fe_{ox1}; Fig. 4). Reducible (crystalline) Fe oxides (Fe_{ox2}) were mostly constant with depth. Sediment Fe sulfide was present as FeS_2 and FeS, with the latter being most abundant at sites LL3A, GOF5, 311, and BY15. Highly reactive Fe accounted for approximately 40% of total Fe at all sites (Fig. S9). The surface sediment was enriched in Mn at sites LL3A, GOF5, BY15, and BY5. At all other sites, surface Mn concentrations were below 14 μmol g^{-1}. At sites LL19 and BY15 concentrations of Fe and Mn were elevated between 5 and 10 cm depth. Elevated ratios of Fe/Al and Mn/Al at the

Table 2. Key site characteristics: Bottom water oxygen (O_2), here based on initial O_2 concentrations in the lander chambers. Organic carbon content in the surface sediment (0–0.5 cm). Oxygen uptake calculated from the change in O_2 concentration in the lander chambers (Fig. S4). Oxygen penetration depth in the sediment (mm) from microprofiles (Fig. S6). Integrated sulfate reduction rates (SRR) are taken from (Hermans et al. 2019*a*) (Fig. S7).

Site	O_2 bottom water (μmol L^{-1})	Organic C (wt%)	O_2 uptake (mmol m^{-2} d^{-1})	O_2 penetration depth (mm)	Integrated SRR (mmol m^{-2} d^{-1})
LL3A	4.8±2.4	10.1	n.a.	n.a.	2.5
GOF5	11.0±1.9	10.4	0.5±0.1	1	2.1
JML	0*	5.8	n.a.	n.a.	1.4
LF1	50.4±3.4	3.5	4.8±0.9	1	0.24
311	3.5±1.4	1.1	n.a.	0	0.57
BY15	1.6	11.4	n.a.	0.05	1.1
LL19	0	9.6	0	n.a.	0.72
BY5	36.2±2.4	5.6	2.6±1	1	1.0
BY2	222.7±14.7	5.8	7.7±3	3.5	0.93

*Bottom water oxygen concentration based on CTD.

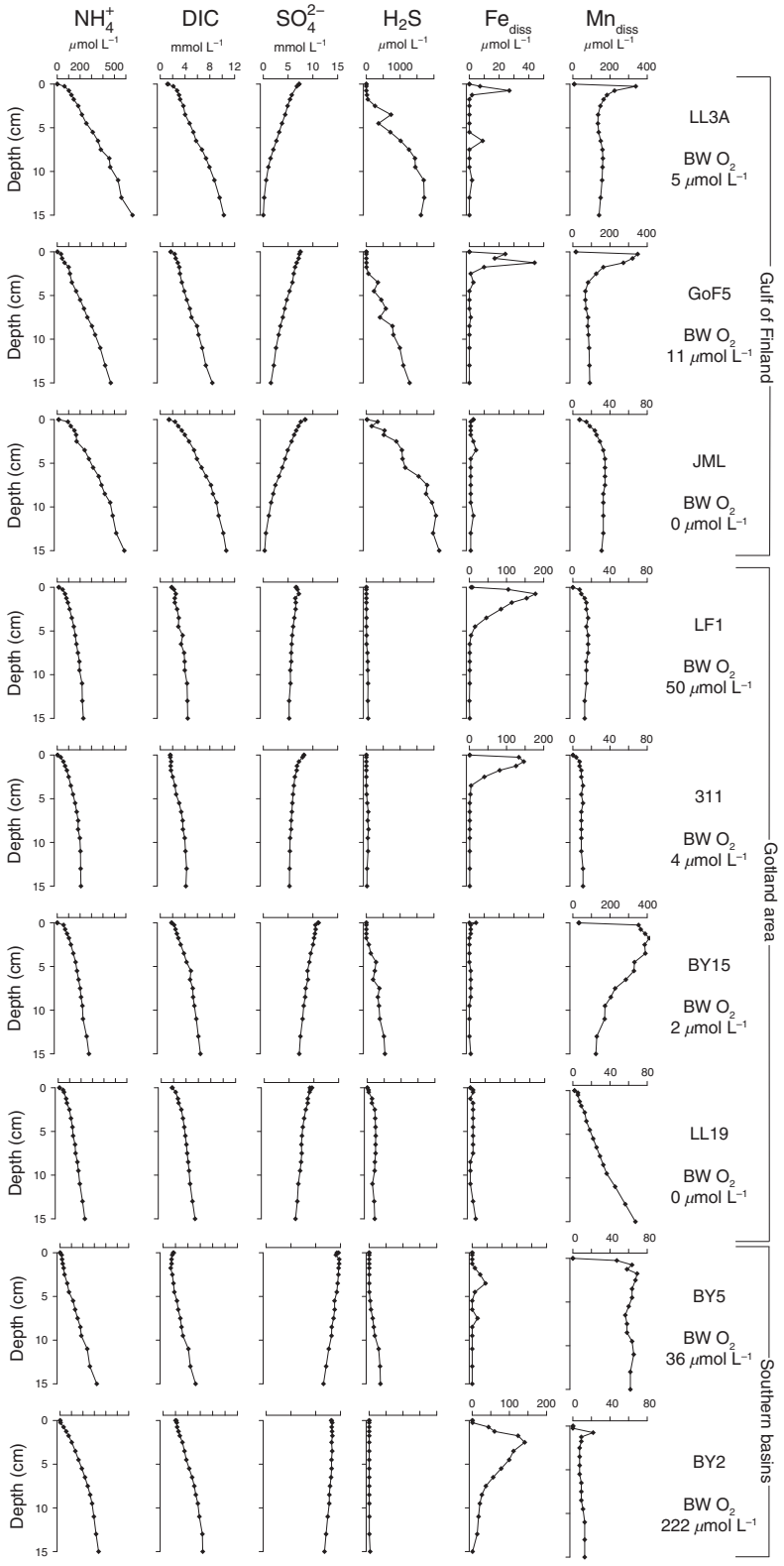

Fig. 2. Porewater depth profiles of NH_4^+, DIC, SO_4^{2-}, H_2S, dissolved Fe and dissolved Mn. Note the different x-axis scale for dissolved Fe at sites LF1, 311, and BY2 and for dissolved Mn at sites LL3A, GOF5, and BY15. Average bottom water oxygen concentrations are given below the label for each station (Table 2). Data points at 0 cm depth are bottom water concentrations.

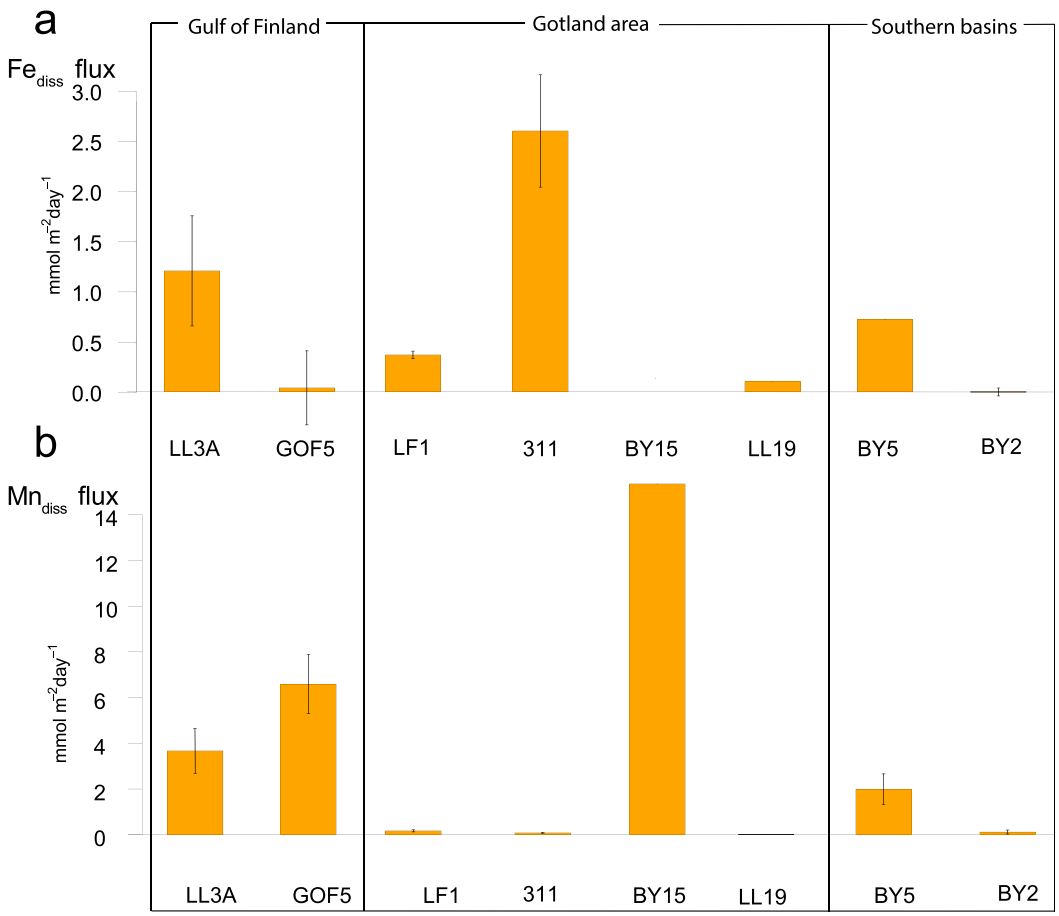

Fig. 3. In situ measured benthic release of (**a**) dissolved Fe and (**b**) dissolved Mn in mmol m^{-2} d^{-1} at eight sites in the Baltic Sea.

sediment water interface were observed at sites LL3A, GOF5, BY15 and BY5. Depth profiles of Fe/Al are similar to depth profiles of Mn/Al at all sites (Fig. 4).

Water column Fe and Mn

Concentrations of aqueous (< 0.02 μm), dissolved (< 0.2 μm) and total Fe were elevated near the seafloor at all sites except site

Table 3. In situ measured and calculated diffusive fluxes based on porewater profiles of dissolved Fe (Fe_{diss}) and dissolved Mn (Mn_{diss}). In situ measurements are average fluxes for all relevant incubation chambers. At sites, LL3A, GoF5, 311, BY5, and BY2 two lander deployments were carried out simultaneously.

Site	Number of Chambers	In situ flux Fe_{diss} (mmol m^{-2} d^{-1})	Diffusive flux Fe_{diss} (mmol m^{-2} d^{-1})	In situ flux Mn_{diss} (mmol m^{-2} d^{-1})	Diffusive flux Mn_{diss} (mmol m^{-2} d^{-1})
LL3A	6	1.21±0.55	0.09	3.7±1.0	4.2
GOF5	6	0.04±0.37	0.31	6.6±1.3	4.2
JML	n.a.	n.a.	−0.002	n.a.	0.09
LF1	3	0.37±0.04	1.14	0.17±0.05	0.08
311	6	2.6±0.56	1.07	0.08±0.02	0.03
BY15	1	n.a.	0.01	15.3	4.5
LL19	3	0.1	0.02	0	0.03
BY5	4	0.72	0	2.0±0.7	0.58
BY2	6	0±0.04	0.18	0.1±0.09	0.9

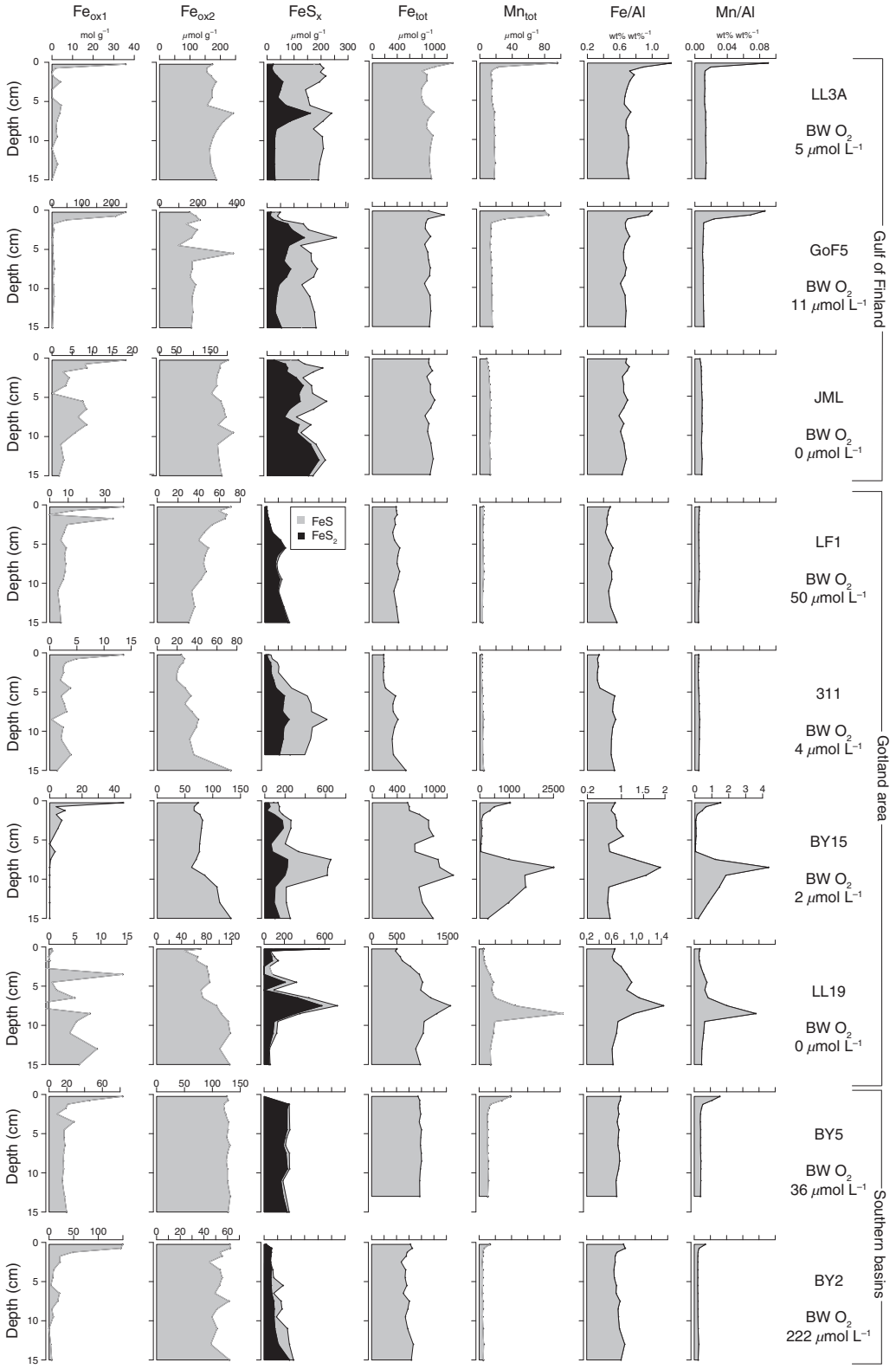

Fig. 4. Solid phase depth profiles of easily reducible Fe oxides (Fe_{ox1}), reducible (crystalline) Fe oxides (Fe_{ox2}), Fe sulfides (FeS in gray and FeS_2 in black), total Fe (Fe_{tot}), total Mn (Mn_{tot}), Fe/Al and Mn/Al at nine sites. Average bottom water oxygen concentrations are given below the label for each station (Table 2).

BY15 (Fig. 5). Depth profiles of aqueous Fe (< 0.02 μm) were similar to those of dissolved Fe (< 0.2 μm; Fig. S10). Distinct differences in concentration ranges between parts of the water column as well as between sites were related to the prevailing redox conditions. At all sites, dissolved and total Fe concentrations were low in the oxic upper part of the water column where they did not exceed 25 and 60 nmol L^{-1}, respectively. In hypoxic waters (at all sites except BY2), dissolved Fe and total Fe concentrations were elevated, ranging up to values of 220 and 1400 nmol L^{-1}, respectively. In the euxinic waters at two sites (JML, LL19), dissolved and total Fe concentrations were similar and ranged up to 2000 nmol L^{-1}. We note, however, that nanoparticulate FeS can pass both a 0.2 and 0.02 μm filter (Wolthers et al. 2003), implying that dissolved and particulate Fe likely are not adequately separated. We assume that most Fe is present as FeS.

For oxic and hypoxic waters enriched in Fe, a distinct contrast in the relative proportion of dissolved vs. particulate Fe (i.e., the difference between total and dissolved Fe) was observed between the three areas. While particulate Fe dominated at the sites in the Gulf of Finland and Southern Basins and accounted for ca. 80–96% of total Fe, this contribution decreased to 25% to 50% at the Gotland area sites. Concentrations of dissolved and total Mn were elevated close to the sediment–water interface at all sites (Fig. 5). Dissolved and total Mn concentrations were low in the oxic upper part of the water column at all sites, where they did not exceed 25 and 120 nmol L^{-1}, respectively. In hypoxic waters, dissolved and total Mn were elevated ranging up to values of 12.4 and 14 μmol L^{-1}, respectively. Concentrations of Mn were high in euxinic waters, with values up to 14 μmol L^{-1}. In oxic and hypoxic waters enriched in Mn, dissolved Mn accounted for most Mn at the sites in the Gulf of Finland and at three of the Gotland area sites. Particulate Mn only dominated over dissolved Mn at site BY15 and at the Southern basin sites.

Concentrations of Fe and Mn in suspended matter as determined with sequential extractions (Fig. 6; Table S1) generally showed the same depth trends as those observed in particulate Fe (Fig. 5). The only exceptions are sites BY2 and BY5, where observed differences were possibly related to spatial variability. Easily reducible Fe and Mn oxides (i.e., ferrihydrite and Mn_{ox1}; Fig. 6), as determined in the first step of the sequential extraction procedure (Table S1) represent the largest fraction of the Fe and Mn extracted from suspended matter.

Discussion

Sediment Fe and Mn dynamics

Mobilization of dissolved Fe and Mn in sediments depends on the input of organic matter and reactive Fe and Mn oxides (Burdige 2006; Lenstra et al. 2019). Our fieldwork areas are characterized by relatively high inputs and rates of degradation of organic matter (e.g., Nilsson et al. (2019)) when compared to other shelf systems (Dale et al. 2015). At our sites, this high rate of organic matter degradation is reflected in shallow oxygen penetration depths and, especially in the Gulf of Finland, elevated porewater concentrations of NH_4^+ and DIC at depth in the sediment (Fig. 2; Table 2). Macrofaunal densities at our sites were generally very low (< 1700 individuals m^{-2}) when compared to other continental shelf areas (e.g., the Black Sea with 6000–10,000 individuals m^{-2}; Lenstra et al. (2019)). Hence, the macrofauna likely had very little impact on the porewater profiles. This is further illustrated by the nearly negligible rates of bioirrigation determined with bromide incubations at sites BY5 and LF1 (Hermans et al. 2019*a*). Low rates of bioirrigation are consistent with previous research showing that benthic communities in the Baltic Sea are naturally constrained by the strong salinity gradients and have been nearly completely eliminated over vast areas due to the low oxygen concentrations in the bottom water (Conley et al. 2009). Despite high rates of organic matter degradation the porewater was not always enriched in dissolved Fe and Mn. Below we discuss the controls on Fe and Mn dynamics in the sediment at our study sites in the Gulf of Finland, Gotland area, and Southern basins.

The Gulf of Finland is the most eutrophic area in the Baltic Sea (Andersen et al. 2015). This is confirmed by our results showing the highest porewater NH_4^+ and DIC concentrations (up to 600 μmol L^{-1} and 10 mmol L^{-1}, respectively (Fig. 2), and high sulfate reduction rates (Table 2; Fig. S7), reflecting high rates of organic input and degradation. At sites LL3A and GOF5, surface sediments are enriched in easily reducible Fe oxides (Fe_{ox1}) and Mn (Fig. 4). The steep decline in Fe_{ox1} and Mn and increase in porewater Fe and Mn with sediment depth reflects rapid reduction of metal oxides below the sediment–water interface (Figs. 2, 4). The relatively low porewater Fe concentrations (< 50 μmol L^{-1}; Fig. 2) for such an Fe oxide-rich sediment with a high rate of organic matter degradation (e.g., Severmann et al. (2010)) are attributed to the high sulfate reduction rates (> 2 mmol m^{-2} d^{-1}; Fig. S7), and associated production of H_2S in the sediment. This leads to excess H_2S over dissolved Fe in the porewater and FeS_x formation (Figs. 2, 4). At site JML, where bottom waters were euxinic at the time of sampling, very little dissolved Fe is present in the porewater, sulfate reduction rates and pore water H_2S are high and almost all Fe is immobilized as FeS_x (Figs. 2, 4, S7). Because the reactivity of dissolved Mn towards H_2S is low, dissolved Mn accumulates in the porewater at all three sites, with the highest concentrations at sites LL3A and GOF5 (up to 400 μmol L^{-1}; Fig. 2). At JML, porewater Mn concentrations were low (Fig. 2), likely because of a low input of Mn oxides.

At our study sites in the Gotland area, porewater concentrations of DIC, NH_4^+, H_2S, and sulfate reduction rates are lower than at those in the Gulf of Finland (Figs. 2 and S7; *t*-test, $p = 0.01$), which is best explained by relatively lower rates of organic matter degradation at the Gotland sites. At the two

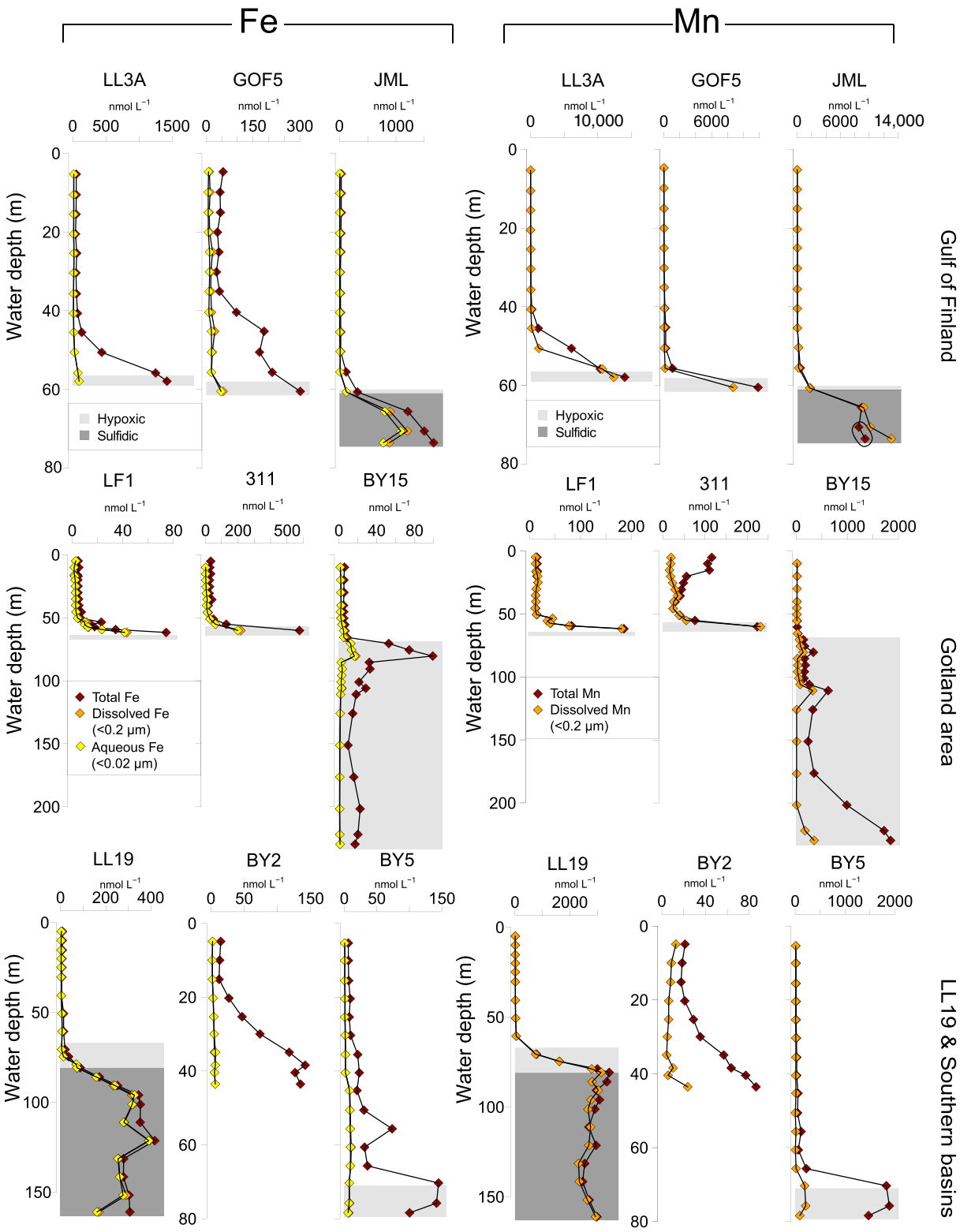

Fig. 5. Water column depth profiles of total and dissolved (< 0.2 μm) Fe and Mn and aqueous Fe (< 0.02 μm) at nine sites in nmol L^{-1}. Light gray areas indicate hypoxic to anoxic bottom water (oxygen = 0–63 μmol L^{-1}), dark gray areas indicate sulfidic conditions. Water column depth profiles of oxygen and H_2S are shown in Fig. S11. Depth profiles of dissolved Fe and aqueous Fe mostly overlap. Total Mn concentrations lower than dissolved Mn concentrations at site JML in sulfidic waters are indicated by a black circle.

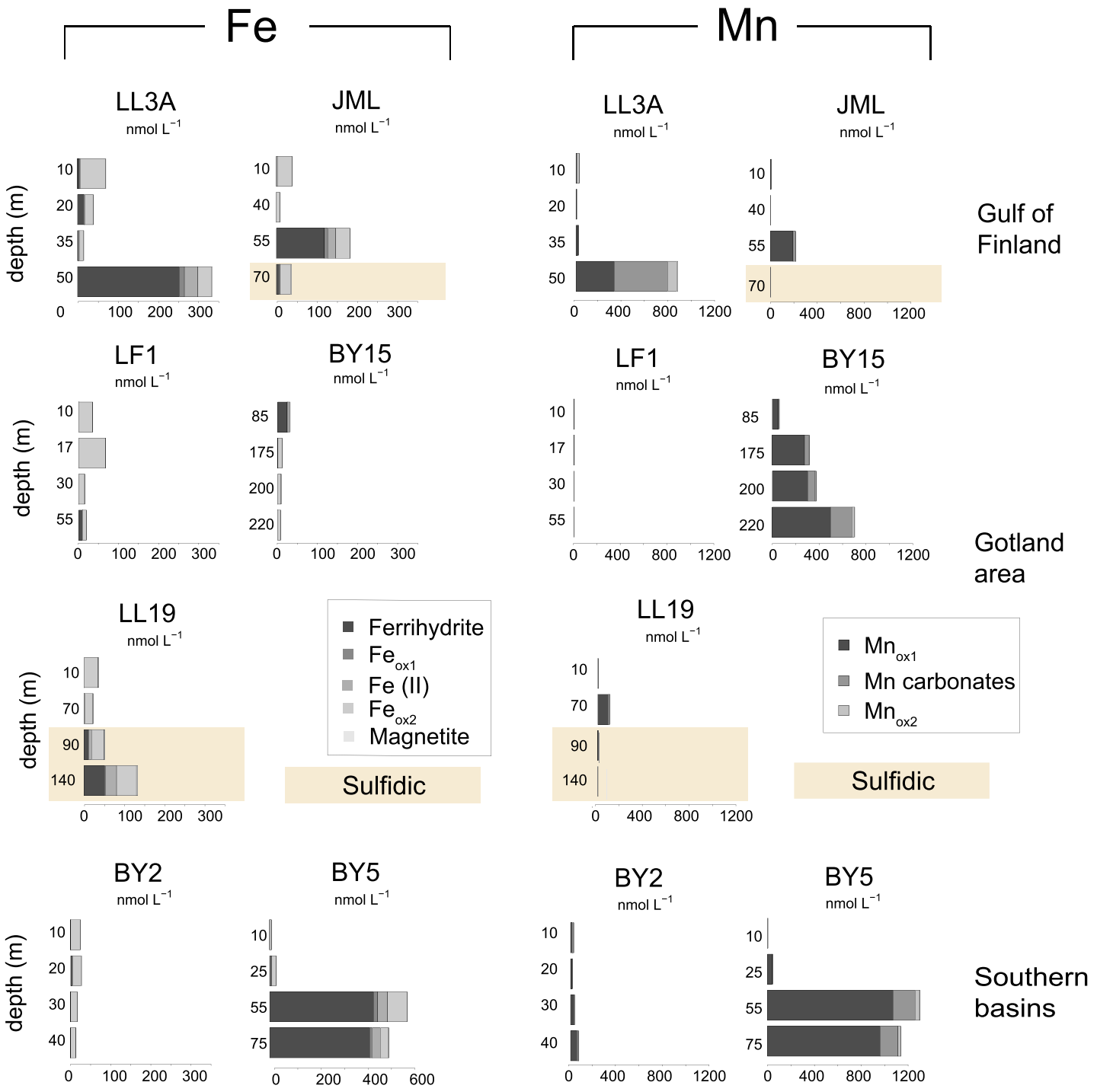

Fig. 6. Forms of Fe and Mn in suspended matter all sites, except for site GOF5 and 311. Data for individual filters are given in Tables S10, S11. For Mn steps 3 and 4 in Table S1 are combined as Mn_{ox2}.

seasonally hypoxic shelf sites (LF1 and 311), there is excess production of dissolved Fe over H_2S, and porewater concentrations of dissolved Fe reach values up to ca. 180 μmol L^{-1}, whereas H_2S concentrations remain below ca. 64 μmol L^{-1} (Fig. 2). Porewater Mn concentrations at these sites are lower (< 80 μmol L^{-1}) than at the Gulf of Finland sites. While the surface sediments are enriched in easily reducible Fe oxides (Fe_{ox1}), there is little Mn (Fig. 4). This low Mn content is in line with earlier observations for this area (Scholz et al. 2013; Lenz et al. 2015*b*). The depletion of Mn relative to Fe is likely

the combined result of (1) the slower oxidation kinetics of Mn(II) with oxygen when compared to Fe(II) (Thamdrup et al. 1994*b*; Stumm and Morgan 1996; Learman et al. 2011) allowing easier escape of dissolved Mn from the sediment and (2) less deposition of reducible Mn oxides when compared to Fe oxides.

At the reoxygenated deep basin site BY15, rates of organic matter degradation are similar to those at site 311 but there is little dissolved Fe in the porewater because of higher H_2S concentrations (up to 500 μmol L^{-1}; Fig. 2). Porewater Mn is elevated because of reduction of Mn oxides near the sediment–water interface. At site LL19, bottom waters are nearly permanently euxinic, resulting in limited deposition of Fe and Mn oxides because of rapid conversion of the Fe oxides to Fe sulfides and dissolution of Mn oxides in the sulfidic waters (Dellwig et al. 2010; Jilbert and Slomp 2013). Porewaters contain negligible dissolved Fe concentrations (Fig. 2) and most Fe is sequestered as FeS_x (Fig. 4), as discussed for JML. There is little recent formation of Mn carbonate due to a lack of sufficient incoming Mn oxide, which is a requirement for the formation in this setting (Jakobsen and Postma 1989; Lenz et al. 2015*b*). The dissolved Mn (up to 70 μmol L^{-1}) at depth in the sediment may have been released from previously formed Mn carbonate layers upon stepwise recrystallization during burial (Jilbert and Slomp 2013).

At the Southern basin sites (BY5 and BY2) both dissolved Fe and Mn are present in the porewater, likely due to dissolution of easily reducible Fe oxides (Fe_{ox1}) and Mn in the surface sediment (Fig. 4). The lower dissolved Fe concentrations at site BY5 when compared to BY2 reflect the higher concentrations of H_2S in the porewater at the former site, which forms upon sulfate reduction (Fig. 2; Table 3). The difference between the average H_2S and dissolved Fe concentrations at BY5 and BY2 is statistically significant (*t*-test, $p = 0.01$).

At sites 311, BY5 and BY2, most porewater Fe (> 75%) was present in colloidal/aqueous form (< 0.2 μm; Fig. S8). This suggests that these fractions dominate the flux of Fe to the overlying water. Further work is needed to elucidate the controls on size fractions of Fe in porewater and the consequences for Fe dynamics in coastal areas.

In summary, these results suggest that differences in H_2S availability in the sediment play a critical role in determining the observed differences in porewater Fe concentrations at our study sites. Highest porewater Fe was observed at sites where the H_2S concentrations were below 5 μmol L^{-1} and the sulfate reduction rate was below 1 mmol m^{-2} d^{-1} (sites: LF1, 311, and BY2; Fig. S7). Porewater Fe was low when H_2S accumulated in the porewater and the sulfate reduction rates were above 1 mmol m^{-2} d^{-1} (sites: LL3A, GOF5, BY15, and BY5). Porewater Mn was elevated at all sites, with the highest concentrations at the seasonally hypoxic sites in the Gulf of Finland (up to 400 μmol L^{-1}) and lowest concentrations at the seasonally hypoxic shelf sites in the Gotland area (below 30 μmol L^{-1}). These contrasts in porewater Mn are at least partly due to differences in Mn oxide supply from the water column at these sites (as discussed in "Water column Fe and Mn dynamics" section).

Benthic release of dissolved Fe and Mn

At our study sites, we observed both high and low rates of benthic release of dissolved Fe and Mn when bottom water oxygen concentrations were below 50 μmol L^{-1} (Fig. 7a,b). This suggests that besides oxygen other factors also control benthic Fe and Mn release. For Fe, dissolved Fe concentrations in the porewater are critical determinants of benthic release. Dissolved Fe is removed when H_2S emerges in the porewater upon depletion of easily reducible Fe oxides (Fig. 2). Hence, the balance between the availability of Fe oxides and H_2S near the sediment–water interface likely determines whether benthic Fe release occurs. The relevant gradient in dissolved Fe that determines the benthic release of Fe cannot be captured with our relatively coarse sampling techniques for porewater. A relationship between the production of H_2S and benthic release of dissolved Fe has been suggested previously based on diagenetic modeling (Wijsman et al. 2001) and sediment records (Scholz et al. 2014).

Benthic release of dissolved Mn at the seasonally hypoxic sites correlates positively with the integrated amount of Mn in the enrichment near the sediment water interface (Fig. 7c). This Mn enrichment was calculated from the total Mn concentrations, corrected for a background concentration, using the measured porosity and a sediment density of 2.65 g cm^{-3} (Burdige 2006). This Mn concentration is assumed to be the Mn in the sediment that is available for benthic Mn release. The correlation suggests that at these sites, the benthic flux of dissolved Mn depends on the availability of reducible Mn oxides. This dependence of benthic Mn release on Mn availability in the sediment is in line with earlier research in the Gulf of Finland and Aarhus Bay, Denmark (Thamdrup et al. 1994*b*; Pakhomova et al. 2007). We find highest benthic release rates of Mn at sites with low bottom water oxygen, in accordance with laboratory experiments and studies for other coastal areas (e.g., Burdige (1993); Sundby et al. (1986); Thamdrup et al. (1994*b*)). We note, however, that in the study of Pakhomova et al. (2007), no relationship between benthic fluxes of Mn and bottom water oxygen was observed for Gulf of Finland sediments. Further research would be needed to explain this difference.

Recently, an empirical function was derived to calculate the benthic flux of dissolved Fe based on bottom water oxygen concentrations and carbon oxidation rates at the global scale (Dale et al. 2015):

$$\text{DFe flux} = \gamma \; tanh\left(\frac{C_{ox}}{O_{2BW}}\right), \quad (1)$$

where DFe flux is the benthic flux of dissolved Fe, C_{ox} is the carbon oxidation rate, O_{2BW} is the bottom water oxygen

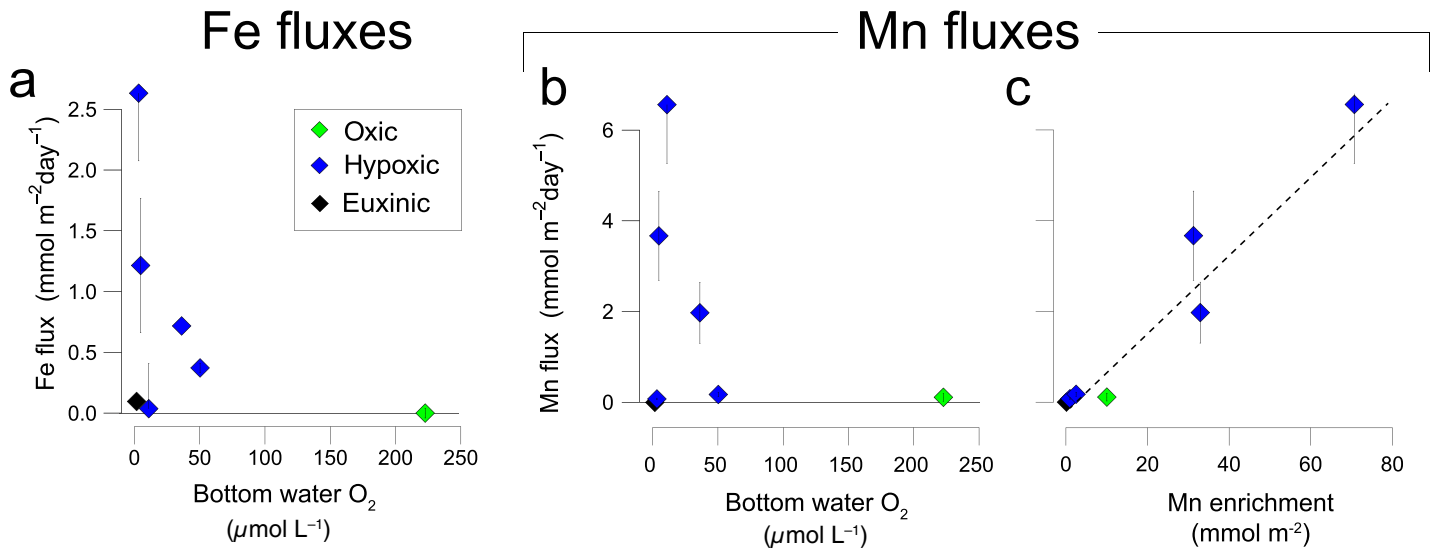

Fig. 7. Benthic release of dissolved Fe vs. (**a**): Bottom water oxygen. Benthic release of dissolved Mn vs. (**b**): Bottom water oxygen and c: Manganese enrichment near the sediment–water interface (mmol m^{-2}). The exceptionally high benthic release of dissolved Mn at site BY15 is not included in figures b and c.

concentration and γ is the maximum flux of dissolved Fe (determined to be 170 μmol m^{-2} d^{-1}; Dale et al. (2015)). Equation (1) thus captures two important controls on benthic release of dissolved Fe for sediments with low macrofaunal activity, as is the case in the open Baltic Sea (Hermans et al. 2019*a*). Generally, the benthic release of dissolved Fe calculated with this model function is in line with observed fluxes of dissolved Fe in open ocean settings. However, the high benthic fluxes of dissolved Fe in river-dominated areas and oxygen minimum zones are not captured by this function (Dale et al. 2015). When applied to our data set, while using typical carbon oxidation rates of Nilsson et al. (2019) for accumulation areas in the Gotland area and Gulf of Finland (32 and 23 mmol m^{-2} d^{-1}, respectively), we find that this model function underestimates the benthic release of Fe: while the maximum flux of Fe predicted by the function is 170 μmol m^{-2} d^{-1}, we observe an up to 15-fold higher flux of Fe at 4 of our sites. Additionally, we show that in highly eutrophic settings high sulfate reduction rates may limit benthic release of dissolved Fe (Fig. 7c), despite low oxygen in the bottom water and high rates of organic carbon oxidation. While the intensity of eutrophication in the Baltic Sea is currently quite exceptional in a global context, more parts of the coastal ocean are expected to become affected by similar processes in future (Reusch et al. 2018). Hence, further refinement of the function of Dale et al. (2015) is needed.

In a recent modeling study, the benthic flux of dissolved Mn was directly coupled to benthic release of dissolved Fe assuming a Fe to Mn ratio of 1 : 5 (van Hulten et al. 2017). At our sites the ratio between benthic Fe/Mn release was highly variable but was mostly below 1 : 1 (Table S13). Sites where high dissolved Mn release was observed differed from sites where dissolved Fe was released (Fig. 3; Table 3). Therefore, benthic release of dissolved Mn should be described by a separate function, including a role for the carbon oxidation rate, bottom water oxygen and Mn availability in the surface sediment.

Water column Fe and Mn dynamics

Benthic fluxes of dissolved Fe and Mn directly impact water column chemistry. In our study, this is most evident for the four seasonally hypoxic sites in the Gulf of Finland and Gotland area. Here, dissolved Fe and Mn concentrations in the bottom water correlate with benthic release of dissolved Fe and Mn (Fig. 8a). However, other factors may also be at play, including dissolved Fe and Mn oxidation to metal oxides in the water column, complexation of Fe and Mn with organic ligands forming dissolved Fe(III)-L and Mn(III)-L (Völker and Tagliabue 2015; Oldham et al. 2017*b*) and lateral supply of Fe- and Mn-bearing waters.

When oxygen is present, dissolved Fe will rapidly oxidize and this likely explains the high percentage of particulate Fe in the water column at most sites (on average, 88% near the seafloor, 81% for all water depths (Figs. 5, 8b). At our study sites, 93% of dissolved Fe in the water column is aqueous Fe (< 0.02 μm) implying that Fe(III)-L plays a minor role (0.02–0.2 μm size fraction; Eckert and Sholkovitz (1976); Schlosser et al. (2013); Oldham et al. (2017*a*)). This suggests that upon precipitation, Fe oxides quickly aggregate to larger particles, in accordance with previous work (Boyle et al. 1977; Lough et al. 2019). Dissolved Mn is not as rapidly oxidized as dissolved Fe and this explains the smaller contribution of particulate Mn to total Mn in the water column (on average 32% near the seafloor, 51% for the whole water column; Figs. 5, 8b)). Complexes of Mn(III)-L, which are smaller in size (< 0.02 μm) and are also suggested to be more stable than

those of Fe(III)-L (Oldham et al. 2017*b*), likely contribute to this dissolved Mn, especially in the upper, oxic water column. In the following section, we will briefly discuss the water column chemistry in each region and the role of the shelf sites as a source of Fe and Mn for deeper areas (Fig. 9).

At the seasonally hypoxic sites in the eutrophic Gulf of Finland (LL3A, GOF5), most Fe near the seafloor is in particulate form (Fig. 5), and ferrihydrite is present in the water column (Fig. 6). For Mn, dissolved Mn is quantitatively more important than particulate Mn, but concentrations of both Mn forms are high (Figs. 5 and 6). In this shelf setting, where bottom waters only recently became hypoxic following the spring oxic period (Hermans et al. 2019*a*), remobilization of dissolved Fe and Mn from sediments likely contributes to the high dissolved and particulate Fe and Mn concentrations in the water column. Part of the Fe and Mn oxides will quickly be redeposited due to gravity-driven settling (e.g., Adelson et al. (2001); Raiswell and Canfield (2012); Sulu-Gambari et al. (2017)). Due to the rapid reduction of Fe and Mn oxides in the sediment, dissolved Fe and Mn is again released to the water column. The resulting refluxing is likely a general feature of many seasonally hypoxic coastal systems, where metal oxides reach the sediment and explains the high total Fe and Mn in the water column in this region (up to 1400 and 14,000 nmol L^{-1}, respectively; Figs. 5, 9). The presence of H_2S and FeS in the water column at site JML suggests it is transitioning from a seasonally hypoxic to a euxinic site (Figs. 5, S11).

In the Gotland area, the range of dissolved and particulate Fe and Mn concentrations in the water column at the seasonally hypoxic shelf sites (LF1, 311) is much lower (580 and 220 nmol L^{-1}, respectively; Fig. 5) than in the Gulf of Finland. Here, nearly all Fe and Mn is in dissolved form. This may be due to the proximity of the chemocline (located at a water depth of ~ 70 m), which is rich in dissolved Fe and Mn (Dellwig et al. 2010) and thus could supply metals to the adjacent shelf edge, as observed in the Black Sea (e.g., Lenstra et al. (2019)). While there is potential for refluxing of Fe between the sediment and water column, there is not for Mn, since there is little particulate Mn in the water column and sediment (Fig. 9).

The two deep basin stations in the Gotland area (BY15, LL19) show contrasting depth profiles of dissolved and particulate Fe and Mn in the water column because of their different location in the basin. At site BY15, the recent inflows resulted in reoxygenation of the deeper waters and the formation of Fe oxides and Mn oxides (birnessite) in the water column (Dellwig et al. 2018; Hermans et al. 2019*b*). The high particulate Mn concentrations near the seafloor are due to Mn refluxing (Dellwig et al. 2018; Hermans et al. 2019*b*). Most Fe is retained in the sediment as FeS_x because of the high porewater concentrations of H_2S close to the sediment–water interface (Hermans et al. 2019*b*). At site LL19, the water column remained euxinic after the inflow because of its more northern position (Hermans et al. 2019*a*), and FeS (which can be smaller than 0.02 μm, and hence will be detected as both "aqueous Fe" and "dissolved Fe") dominates the Fe-pool in the water column. Most Mn is present in dissolved form, as is typical for euxinic waters (Fig. 9).

At the Southern basin sites (BY2, BY5), most Fe and Mn near the seafloor is present in particulate form (Figs. 5, 6). Bottom waters at both sites are relatively high in bottom water oxygen (Table 2) for the time of the year because of the recent North Sea inflow (Hermans et al. 2019*a*). At BY5 the combined

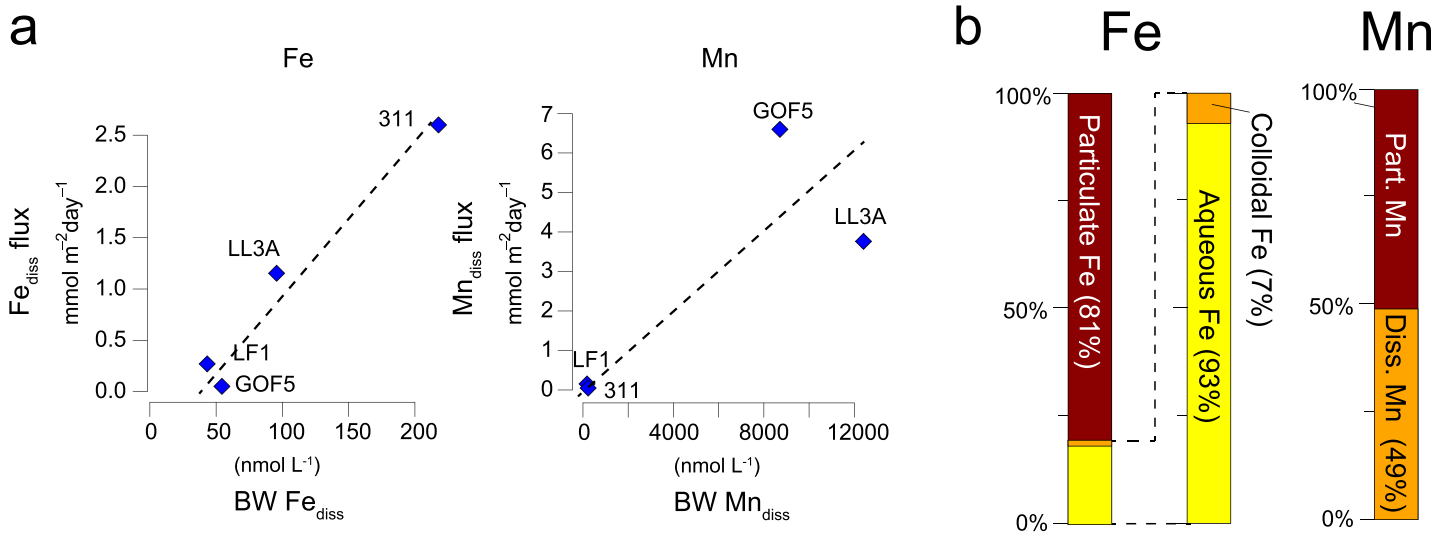

Fig. 8. (**a**) Correlation between benthic release of dissolved Fe and Mn, and bottom water dissolved Fe and Mn (BW Fe_{diss} and BW Mn_{diss}) for sites LL3A, GOF5, LF1 and 311. (**b**) Average contribution of particulate (> 0.2 μm), colloidal (0.02–0.2 μm) and aqueous (< 0.02 μm) Fe and particulate and dissolved Mn in the entire water column at all sites.

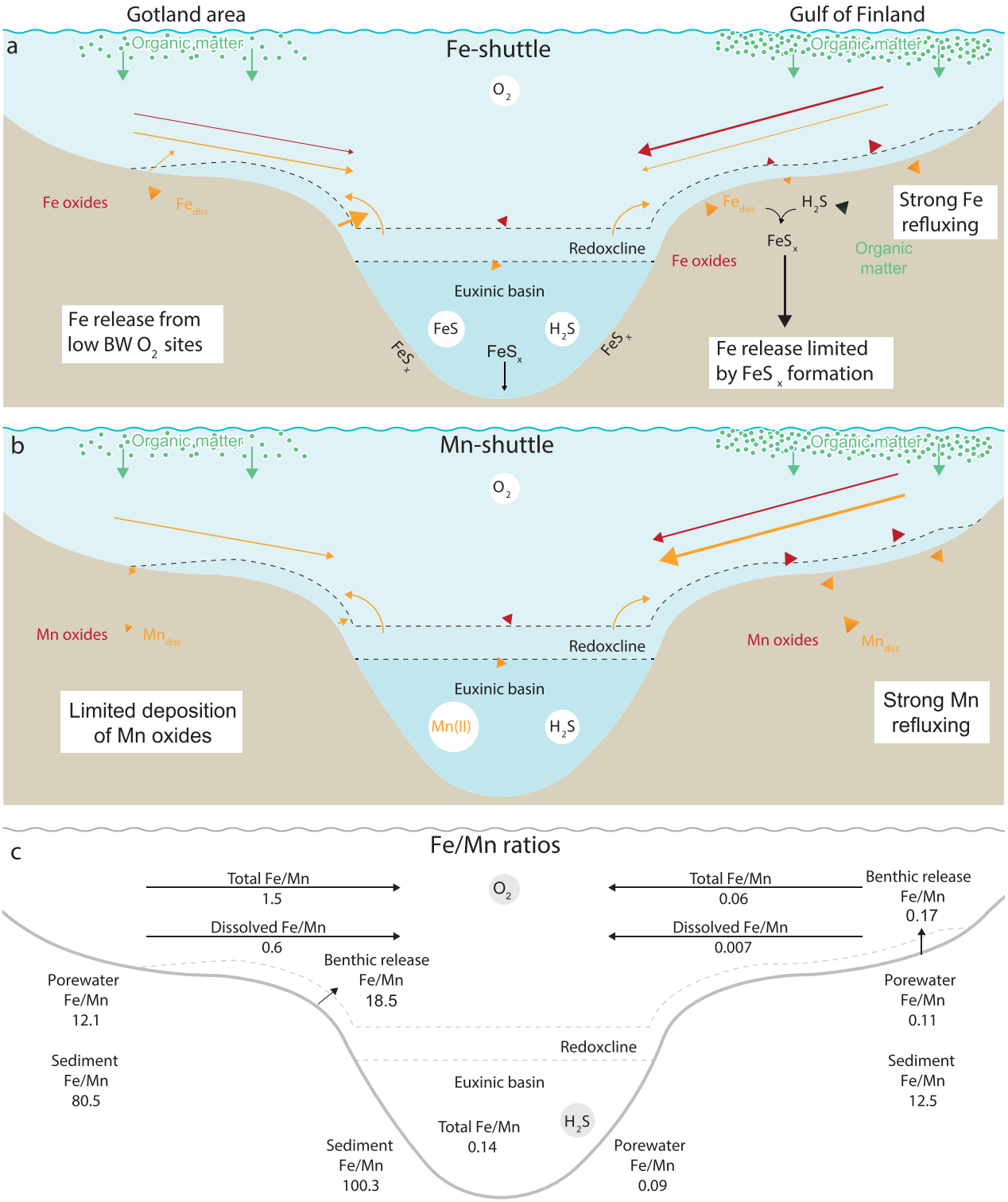

Fig. 9. Schematic overview of the Gotland area and Gulf of Finland (**a**) Fe shuttling; (**b**) Mn shuttling. (**c**) Ratio of Fe/Mn in the Baltic Sea; ratios were calculated by averaging over two stations in the Gulf of Finland (LL3A and GOF5) and Gotland area (LF1 and 311). Porewater Fe/Mn was calculated from the maximum concentrations in the first 15 cm. Water column total and dissolved Fe/Mn were calculated for the lowest sample in the water column. Sediment Fe/Mn was calculated at the sediment–water interface (0–0.5 cm). Water column and sediment Fe/Mn ratios in the euxinic basin were averaged for sites JML and LL19.

porewater, benthic flux and water column data suggest refluxing of both Fe and Mn, but without reaching the same benthic release fluxes as in the Gulf of Finland (Figs. 2, 3, 5, 6).

From the above, it follows that the quantitative contribution of particulate vs. dissolved forms of Fe and Mn in areas sampled in the Baltic Sea depends strongly on bottom water redox conditions, porewater concentrations of H_2S and the proximity to the chemocline. Lateral transfer of water and suspended matter will also play a role by determining the residence time of the water in each area and by influencing the rate of transport of Fe and Mn in suspended and dissolved form to the deep basins. Our results suggest that the Gulf of Finland could potentially supply both Fe and Mn to the deep basin waters in the Baltic proper. The low total Fe/Mn ratio in the bottom waters of the Gulf of Finland (0.06; Fig. 9) reflects the higher mobility and availability of Mn when compared to Fe. The bottom waters on the shelf of the Gotland area, in contrast, are characterized by waters with a much higher total Fe/Mn ratio (1.5; Fig. 9), reflecting the much lower availability of Mn (and not a much higher Fe availability) in this region when compared to the Gulf of Finland and hence less important role as a Mn source.

In the euxinic waters of the deep basins, Mn remains in dissolved form, while most Fe is likely captured as FeS_x (e.g., JML and LL19, Figs. 4, 5, 9; Dyrssen and Kremling (1990)). With the expansion of the euxinic waters in the Baltic Sea, the ratio of the area of the seafloor that acts as a source and as a sink for Fe and Mn shuttling has decreased in the last decades (Anderson and Raiswell 2004; Jilbert and Slomp 2013). Some of the sediment sources are (partly) depleted, as evidenced by the low sediment Mn concentrations on the shelf in the Gotland area (Fig. 9) and by low sediment Fe in some locations (Scholz et al. 2013). At euxinic site LL19 and recently reoxygenated (but otherwise euxinic) site BY15, maximum Fe/Al ratios occur between 5 to 10 cm sediment depth (Fig. 4). The lack of high Fe/Al in the surface sediments at these two Baltic sites reflects less efficient Fe shuttling to the Gotland basin following the recent expansion of hypoxia (e.g., Reed et al. (2016)), as observed in other marine systems (Raiswell and Canfield 2012)). Since the present-day Fe burial flux is similar to that prior to the onset hypoxia (Lenz et al. 2015*a*; Reed et al. 2016), this suggests that little of the Fe that is currently mobilized in the seasonally hypoxic areas of the Gulf of Finland is transported to the deep basins in the Gotland area. The most likely explanation is that it is retained as FeS_x in the western part of the Gulf of Finland.

Implications

The Baltic Sea is highly eutrophic and hosts an unusually large low oxygen area, making it an extreme end member when compared to other modern coastal systems subject to deoxygenation (Reusch et al. 2018). We find maximum benthic release rates of Fe of up to 2.6 mmol m^{-2} d^{-1}, which are one order of magnitude higher than those in other coastal systems (Fig. 7; Dale et al. (2015)). Benthic Mn fluxes reach values of up to 15.2 mmol m^{-2} d^{-1}, where for other coastal areas rates often remain below 0.5 mmol m^{-2} d^{-1} (e.g., Johnson et al. (1992); Thamdrup et al. (1994a)). The high fluxes of Fe and Mn observed for the Gulf of Finland are not unique to this study and were also observed by Pakhomova et al. (2007). Importantly, the Baltic Sea sediments studied here are not subject to an unusually high external Fe or Mn oxide supply nor are they characterized by unusually high sediment contents of reactive and total Fe and Mn when compared to other coastal systems (Fig. 4; Slomp et al. (1997); Lyons and Severmann (2006)). Instead, we propose that strong Fe and/or Mn refluxing is responsible for the surface enrichments in sediment Fe and Mn and the high benthic release fluxes. Such a mechanism was proposed earlier by Lohan and Bruland (2008) to explain high dissolved Fe on the hypoxic shelf off Oregon and Washington. Here, we show that eutrophication greatly amplifies Fe and Mn refluxing, by promoting rapid dissolution of reducible Fe and Mn oxides near the sediment surface. The rate of refluxing benefits from a shallow hypoxic layer (< 6 m), since this will reduce the time needed for upward diffusive and turbulent transfer of dissolved Fe and Mn into oxic waters and downward, gravity-driven settling of metal oxides. For Fe, the lack of H_2S in the bottom water and surface sediment, as observed at our sites (Figs. 2, S11), is critical to allow high Fe fluxes to be maintained. For Mn, the supply of Mn oxides can become limiting because of the higher mobility and solubility of dissolved Mn. The observation that Fe and Mn refluxing can occur in a relatively open coastal setting without the need for an unusually high external Fe and Mn input, implies that this mechanism could also become active at sites with fine-grained, sulfidic sediments in eutrophic areas on continental shelves. An example of such an area is the Helgoland Bight in the North Sea (Slomp et al. 1997). Similar muddy areas on other continental shelves could become seasonal hotspots for dissolved Fe and Mn release to the overlying water upon eutrophication and deoxygenation of their bottom waters.

Our findings also confirm the "redox window" for release of Fe from continental shelves as deduced from sediment records (Scholz et al. 2014; Lenz et al. 2015*a*). This non-linear behavior of benthic Fe release is currently not included in empirical models used to predict Fe fluxes in global models (Elrod et al. 2004; Dale et al. 2015). Our results highlight that multiple factors control benthic fluxes of Fe and Mn and that, besides bottom water oxygen and carbon oxidation rates, the availability of H_2S in the porewater (for Fe) and Mn oxide supply (for Mn) could be relevant. Further work is needed to improve current empirical functions for benthic Fe and Mn release from shelf sediments. This requires field and modeling studies combining in situ benthic flux measurements of Fe and Mn and detailed analyses of the corresponding sediment

geochemistry (preferably including measurements of rates of reactions) for a wide range of shelf environments.

References

Adelson, J. M., G. R. Helz, and C. V. Miller. 2001. Reconstructing the rise of recent coastal anoxia; molybdenum in Chesapeake Bay sediments. Geochimica et Cosmochimica Acta **65**: 237–252.

Andersen, J. H., et al. 2015. Long-term temporal and spatial trends in eutrophication status of the Baltic Sea. Biological Reviews **92**: 135–149.

Anderson, T. F., and R. Raiswell. 2004. Sources and mechanisms for the enrichment of highly reactive iron in euxinic Black Sea sediments. American Journal of Science **304**: 203–233.

APHA (2005). Standard methods for the examination of water and wastewater. American Public Health Association.

Berelson, W., and others. 2003. A time series of benthic flux measurements from Monterey Bay, CA. Continental Shelf Research **23**: 457–481.

Berner, R. A. 1984. Sedimentary pyrite formation: An update. Geochimica et Cosmochimica Acta **48**: 605–615.

Boyle, E. A., J. M. Edmond, and E. R. Sholkovitz. 1977. The mechanism of iron removal in estuaries. Geochimica et Cosmochimica Acta **41**: 1313–1324.

Breitburg, D., and others. 2018. Declining oxygen in the global ocean and coastal waters. Science **359**: eaam7240.

Brewer, P. G., and D. W. Spencer. 1971. Colorimetric determination of manganese in anoxic waters. Limnology and Oceanography **16**: 107–110.

Burdige, D. J. 1993. The biogeochemistry of manganese and iron reduction in marine sediments. Earth Science Reviews **35**: 249–284.

Burdige, D. J. 2006. Geochemistry of Marine Sediments. Princeton University Press. http://dx.doi.org/10.1086/533614

Burton, E. D., R. T. Bush, and L. A. Sullivan. 2006. Fractionation and extractability of sulfur, iron and trace elements in sulfidic sediments. Chemosphere **64**: 1421–1428.

Claff, S. R., L. A. Sullivan, E. D. Burton, and R. T. Bush. 2010. A sequential extraction procedure for acid sulfate soils: Partitioning of iron. Geoderma **155**: 224–230.

Conley, D. J., and others. 2009. Hypoxia-related processes in the Baltic Sea. Environmental Science and Technology **43**: 3412–3420.

Dale, A. W., L. Nickelsen, F. Scholz, C. Hensen, A. Oschlies, and K. Wallmann. 2015. A revised global estimate of dissolved iron fluxes from marine sediments. Global Biogeochemical Cycles **29**: 691–707.

Dellwig, O., T. Leipe, C. März, M. Glockzin, F. Pollehne, B. Schnetger, E. V. Yakushev, M. E. Böttcher, and H. J. Brumsack. 2010. A new particulate Mn-Fe-P-shuttle at the redoxcline of anoxic basins. Geochimica et Cosmochimica Acta **74**: 7100–7115.

Dellwig, O., B. Schnetger, D. Meyer, F. Pollehne, K. Häusler, and H. W. Arz. 2018. Impact of the Major Baltic inflow in 2014 on manganese cycling in the Gotland deep (Baltic Sea). Frontiers in Marine Science **5**: 248.

Diaz, R. J., and R. Rosenberg. 2008. Spreading dead zones and consequences for marine ecosystems. Science **321**: 926–929.

Dyrssen, D., and K. Kremling. 1990. Increasing hydrogen sulfide concentration and trace metal behavior in the anoxic Baltic waters. Marine Chemistry **30**: 193–204.

Eckert, J. M., and E. R. Sholkovitz. 1976. The flocculation of iron, aluminium and humates from river water by electrolytes. Geochimica et Cosmochimica Acta **40**: 847–848.

Elrod, V. A., W. M. Berelson, K. H. Coale, and K. S. Johnson. 2004. The flux of iron from continental shelf sediments: A missing source for global budgets. Geophysical Research Letters **31**: 2–5.

Emerson, S., S. Kalhorn, L. Jacobs, B. M. Tebo, K. H. Nealson, and R. A. Rosson. 1982. Environmental oxidation rate of manganese(II): Bacterial catalysis. Geochimica et Cosmochimica Acta **46**: 1073–1079.

Fossing, H., and B. B. Jørgensen. 1989. Measurement of bacterial sulfate reduction in sediments: Evaluation of a single-step chromium reduction method. Biogeochemistry **8**: 205–222.

Gledhill, M., and C. M. G. van den Berg. 1994. Determination of complexation of iron(III) with natural organic complexing ligands in seawater using cathodic stripping voltammetry. Marine Chemistry **47**: 41–54.

Grasshoff, K., K. Kremling, and M. Ehrhardt. 2009. Methods of seawater analysis. John Wiley & Sons. https://doi.org/10.1016/0304-4203(78)90045-2

Heiser, U., T. Neumann, J. Scholten, and D. Stüben. 2001. Recycling of manganese from anoxic sediments in stagnant basins by seawater inflow: A study of surface sediments from the Gotland Basin, Baltic Sea. Marine Geology **177**: 151–166.

Hermans, M., W. K. Lenstra, S. Hidalgo-Martinez, N. A. G. M. van Helmond, R. Witbaard, F. J. Meysman, S. Gonzalez, and C. P. Slomp. 2019*a*. Abundance and biogeochemical impact of cable bacteria in Baltic Sea sediments. Environmental Science & Technology **53**: 7494–7503.

Hermans, M., W. K. Lenstra, N. A. G. M. van Helmond, T. Behrends, M. Egger, M. J. M. Séguret, E. Gustafsson, B. G. Gustafsson, and C. P. Slomp. 2019*b*. Impact of natural reoxygenation on the sediment dynamics of manganese, iron and phosphorus in a euxinic Baltic Sea basin. Geochimica et Cosmochimica Acta **246**: 174–196.

Homoky, W. B., D. J. Hembury, L. E. Hepburn, R. a. Mills, P. J. Statham, G. R. Fones, and M. R. Palmer. 2011. Iron and manganese diagenesis in deep sea volcanogenic sediments and the origins of pore water colloids. Geochimica et Cosmochimica Acta **75**: 5032–5048.

Jakobsen, R., and D. Postma. 1989. Formation and solid solution behavior of Ca-rhodochrosites in marine muds of the Baltic deeps. Geochimica et Cosmochimica Acta **53**: 2639–2648.

Jilbert, T., and C. P. Slomp. 2013. Iron and manganese shuttles control the formation of authigenic phosphorus minerals in the euxinic basins of the Baltic Sea. Geochimica et Cosmochimica Acta **107**: 155–169.

Johnson, K. S., W. M. Berelson, K. H. Coale, T. L. Coley, V. A. Elrod, W. R. Fairey, H. D. Iams, T. E. Kilgore, and J. L. Nowicki. 1992. Manganese flux from continental margin sediments in a transect through the oxygen minimum. Science **257**: 1242–1245.

Klunder, M. B., P. Laan, R. Middag, H. J. W. De Baar, and J. C. van Ooijen. 2011. Dissolved iron in the Southern Ocean (Atlantic sector). Deep-Sea Research Part II: Topical Studies in Oceanography **58**: 2678–2694.

Koroleff, F. 1970. Direct determination of ammonia in natural waters as indophenol blue. Information on Techniques and Methods for Seawater Analysis, 19–22.

Kraal, P., C. P. Slomp, A. Forster, M. M. M. Kuypers, and A. Sluijs. 2009. Pyrite oxidation during sample storage determines phosphorus fractionation in carbonate-poor anoxic sediments. Geochimica et Cosmochimica Acta **73**: 3277–3290.

Kraal, P., N. Dijkstra, T. Behrends, and C. P. Slomp. 2017. Phosphorus burial in sediments of the sulfidic deep Black Sea: Key roles for adsorption by calcium carbonate and apatite authigenesis. Geochimica et Cosmochimica Acta **204**: 140–158.

Lagerström, M. E., M. P. Field, M. Séguret, L. Fischer, S. Hann, and R. M. Sherrell. 2013. Automated on-line flow-injection ICP-MS determination of trace metals (Mn, Fe, Co, Ni, Cu and Zn) in open ocean seawater: Application to the GEOTRACES program. Marine Chemistry **155**: 71–80.

Learman, D. R., B. M. Voelker, A. I. Vazquez-Rodriguez, and C. M. Hansel. 2011. Formation of manganese oxides by bacterially generated superoxide. Nature Geoscience **4**: 95–98.

Lenstra, W. K., and others. 2019. The shelf-to-basin iron shuttle in the Black Sea revisited. Chemical Geology **511**: 314–341.

Lenstra, W. K., M. J. M. Séguret, T. Behrends, R. K. Groeneveld, M. Hermans, R. Witbaard, and C. P. Slomp. 2020. Controls on the shuttling of manganese over the northwestern Black Sea shelf and its fate in the euxinic deep basin. Geochimica et Cosmochimica Acta **273**: 177–204.

Lenz, C., T. Jilbert, D. J. Conley, and C. P. Slomp. 2015*a*. Hypoxia-driven variations in iron and manganese shuttling in the Baltic Sea over the past 8 kyr. Geochemistry, Geophysics, Geosystems **16**: 3754–3766.

Lenz, C., T. Jilbert, D. J. Conley, M. Wolthers, and C. P. Slomp. 2015*b*. Are recent changes in sediment manganese sequestration in the euxinic basins of the Baltic Sea linked to the expansion of hypoxia? Biogeosciences **12**: 4875–4894.

Lohan, M. C., and K. W. Bruland. 2008. Elevated Fe(II) and dissolved Fe in hypoxic shelf waters off Oregon and Washington: An enhanced source of iron to coastal upwelling regimes. Environmental Science and Technology **42**: 6462–6468.

Lough, A. J. M., W. B. Homoky, D. P. Connelly, K. Nakamura, M. K. Abyaneh, B. Kaulich, and R. A. Mills. 2019. Soluble iron conservation and colloidal iron dynamics in a hydrothermal plume. Chemical Geology **511**: 225–237.

Lyons, T. W., and S. Severmann. 2006. A critical look at iron paleoredox proxies: New insights from modern euxinic marine basins. Geochimica et Cosmochimica Acta **70**: 5698–5722.

Millero, F. J., S. Sotolongo, and M. Izaguirre. 1987. The oxidation kinetics of Fe(II) in seawater. Geochimica et Cosmochimica Acta **51**: 793–801.

Mohrholz, V., M. Naumann, G. Nausch, S. Krüger, and U. Gräwe. 2015. Fresh oxygen for the Baltic Sea - an exceptional saline inflow after a decade of stagnation. Journal of Marine Systems **148**: 152–166.

Moore, C. M., and others. 2013. Processes and patterns of oceanic nutrient limitation. Nature Geoscience **6**: 701–710.

Nilsson, M. M., and others. 2019. Organic carbon recycling in Baltic Sea sediments–an integrated estimate on the system scale based on in situ measurements. Marine Chemistry **209**: 81–93.

Noble, A. E., and others. 2012. Basin-scale inputs of cobalt, iron, and manganese from the Benguela-Angola front to the South Atlantic Ocean. Limnology and Oceanography **57**: 989–1010.

Oldham, V. E., M. T. Miller, L. T. Jensen, and G. W. Luther. 2017*a*. Revisiting Mn and Fe removal in humic rich estuaries. Geochimica et Cosmochimica Acta **209**: 267–283.

Oldham, V. E., A. Mucci, B. M. Tebo, and G. W. Luther. 2017*b*. Soluble Mn(III)L complexes are abundant in oxygenated waters and stabilized by humic ligands. Geochimica et Cosmochimica Acta **199**: 238–246.

Pakhomova, S. V., P. O. J. Hall, M. Y. Kononets, A. G. Rozanov, A. Tengberg, and A. V. Vershinin. 2007. Fluxes of iron and manganese across the sediment-water interface under various redox conditions. Marine Chemistry **107**: 319–331.

Poulton, S. W., and D. E. Canfield. 2005. Development of a sequential extraction procedure for iron: Implications for iron partitioning in continentally derived particulates. Chemical Geology **214**: 209–221.

Raiswell, R., and D. E. Canfield. 2012. The iron biogeochemical cycle past and present. Geochemical Perspectives **1**: 1–220.

Raiswell, R., H. P. Vu, L. Brinza, and L. G. Benning. 2010. The determination of labile Fe in ferrihydrite by ascorbic acid

extraction: Methodology, dissolution kinetics and loss of solubility with age and de-watering. Chemical Geology **278**: 70–79.

Reed, D. C., B. G. Gustafsson, and C. P. Slomp. 2016. Shelf-to-basin iron shuttling enhances vivianite formation in deep Baltic Sea sediments. Earth and Planetary Science Letters **434**: 241–251.

Reusch, T. H. B., and others. 2018. The Baltic Sea as a time machine. Science Advances **4**: eaar8195.

Rijkenberg, M. J. A., and others. 2015. "PRISTINE", a new high volume sampler for ultraclean sampling of trace metals and isotopes. Marine Chemistry **177**: 501–509.

Schlosser, C., P. Streu, and P. L. Croot. 2013. Vivaspin ultrafiltration: A new approach for high resolution measurements of colloidal and soluble iron species. Limnology and Oceanography: Methods **11**: 187–201.

Scholz, F., J. McManus, and S. Sommer. 2013. The manganese and iron shuttle in a modern euxinic basin and implications for molybdenum cycling at euxinic ocean margins. Chemical Geology **355**: 56–68.

Scholz, F., J. McManus, A. C. Mix, C. Hensen, and R. R. Schneider. 2014. The impact of ocean deoxygenation on iron release from continental margin sediments. Nature Geoscience **7**: 433–437.

Severmann, S., J. McManus, W. M. Berelson, and D. E. Hammond. 2010. The continental shelf benthic iron flux and its isotope composition. Geochimica et Cosmochimica Acta **74**: 3984–4004.

Slomp, C., J. Malschaert, L. Lohse, and W. Van Raaphorst. 1997. Iron and manganese cycling in different sedimentary environments on the North Sea continental margin. Continental Shelf Research **17**: 1083–1117.

Soetaert, K., T. Petzoldt, and F. J. R. Meysman. 2010. Marelac: tools for aquatic sciences v2.1.3. *R package*. https://cran.r-project.org/web/packages/marelac/vignettes/marelac.pdf

Stoll, M. H. C., K. Bakker, G. H. Nobbe, and R. R. Haese. 2001. Continous-flow analysis of dissolved inorganic carbon content in seawater. Analytical Chemistry **73**: 4111–4116.

Stumm, W., and J. J. Morgan. 1996. Aquatic chemistry: Chemical Equilibria and rates in natural waters. John Wiley & Sons. https://doi.org/10.1016/S0016-7037(97)81133-7

Sulu-Gambari, F., A. Roepert, T. Jilbert, M. Hagens, F. J. R. Meysman, and C. P. Slomp. 2017. Molybdenum dynamics in sediments of a seasonally-hypoxic coastal marine basin. Chemical Geology **466**: 627–640.

Sundby, B., L. G. Anderson, P. O. J. Hall, Å. Iverfeldt, M. M. R. van der Loeff, and S. F. G. Westerlund. 1986. The effect of oxygen on release and uptake of cobalt, manganese, iron and phosphate at the sediment-water interface. Geochimica et Cosmochimica Acta **50**: 1281–1288.

Thamdrup, B., H. Fossing, and B. B. Jørgensen. 1994*a*. Manganese, iron and sulfur cycling in a coastal marine sediment, Aarhus bay, Denmark. Geochimica et Cosmochimica Acta **58**: 5115–5129.

Thamdrup, B., R. N. Glud, and J. W. Hansen. 1994*b*. Manganese oxidation and in situ manganese fluxes from a coastal sediment. Geochimica et Cosmochimica Acta **58**: 2563–2570.

van Hulten, M. M. P., R. Middag, J. C. Dutay, H. J. W. de Baar, M. Roy-Barman, M. Gehlen, A. Tagliabue, and A. Sterl. 2017. Manganese in the West Atlantic Ocean in context of the first global ocean circulation model of manganese. Biogeosciences **14**: 1123–1152.

Völker, C., and A. Tagliabue. 2015. Modeling organic iron-binding ligands in a three-dimensional biogeochemical ocean model. Marine Chemistry **173**: 67–77.

Wijsman, J. W. M., J. J. Middelburg, and C. H. R. Heip. 2001. Reactive iron in Black Sea sediments: Implications for iron cycling. Marine Geology **172**: 167–180.

Wolthers, M., S. J. Van Der Gaast, and D. Rickard. 2003. The structure of disordered mackinawite. American Mineralogist **88**: 2007–2015.

Acknowledgments

We thank the captain, crew, technicians, Niels van Helmond, Amy Kuzminov and Matthias Egger aboard R/V *Pelagia* in June 2016 for their assistance and Helen de Waard, Coen Mulder, Arnold van Dijk and Reinier Groeneveld for analytical assistance in Utrecht. We thank two reviewers for insightful comments that improved the manuscript. This research was funded by NWO-Vici grant 865.13.005 (to CPS).

Conflict of interest

None declared.

Submitted 12 February 2020
Revised 09 July 2020
Accepted 14 October 2020

Associate editor: Maria Maldonado